Designing a Planar T-match Antenna to have a 2nd-order Chebyshev Band-Pass Filter Frequency Response for the Purpose of UHF RFID

by

Thomas Northup

Submitted to the graduate degree program in Electrical Engineering and Computer Science and the Graduate Faculty of the University of Kansas in partial fulfillment of the requirements for the degree of Master of Science.

_____

Chairperson: Dr. Kenneth Demarest

_____

Dr. Daniel Deavours

_____

Dr. James Stiles

Date Defended: August 30, 2011

The Thesis Committee for Thomas Northup certifies

that this is the approved version of the following thesis:

Designing a Planar T-match Antenna to have a 2nd-order Chebyshev Band-Pass Filter Frequency Response for the Purpose of UHF RFID

_____

Chairperson: Dr. Kenneth Demarest

_____

Dr. Daniel Deavours

_____

Dr. James Stiles

Date approved: September 2, 2011

Abstract

Radio Frequency Identification (RFID) uses radio communication to identify physical objects that have transponders attached. Supply chain management is one of the main applications that has pushed the development of these transponders, called tags, over the last two decades. The T-match antenna is a common antenna type used by engineers designing RFID tags. To make T-match-based RFID tags more efficient at wider bandwidths, their power transfer efficiency (PTE) frequency responses have been designed to match those of band-pass filters that meet the user's desired frequency requirements. In this thesis, the equivalent circuit of the T-match antenna is shown to have the same form as a 2nd-order band-pass filter, and an existing RFID tag antenna's response is redesigned to match that of a 2nd-order Chebyshev filter. Three antenna designs are simulated that greatly increased the bandwidths over conventional T-match design procedures. This increased bandwidth can potentially allow the RFID tags using these antennas to be read at longer distances, or allow the power needed to read them at a particular distance to be reduced.

Acknowledgements

I thank Dr. Demarest for his guidance in my thesis work and my education at The University of Kansas. As a graduate advisor he has been patient with me while helping me make the most of my thesis and graduate education. He has challenged me in the development of my person and skills to strive for the highest professional standards. I have learned much from having him for a professor for several courses in my college career and have benefited from his insights.

I thank Dr. Deavours for his knowledge and guidance in the field of Radio Frequency Identification (RFID). His perspectives and insights have given me a much broader understanding of the RFID field and a better understanding of different ways to approach problems within the RFID field. I also thank Dr. Stiles for his willingness to be a part of my thesis committee, and for the knowledge and guidance I received from taking several courses from him. I thank Instructor Lagotte with The University of Kansas Graduate Writing Program for helping me develop my writing skills for this thesis.

I thank the Electrical Engineering and Computer Science Department at The University of Kansas for the support of its professors and staff in my college career. I also thank the Information and Telecommunication Technology Center for allowing me use of their resources while working on my thesis.

Finally, I thank my family and friends for their love and support during my college career and especially during my thesis work. They have aided and encouraged me at times when I needed it most.

Table of Contents

1. Introduction

Radio Frequency Identification (RFID) identifies physical objects using radio communications. RFID can use a variety of technologies and techniques depending on the specific application and the frequency it uses for radio communication. The basic configuration for a typical RFID system includes a transmitter-receiver, often called a reader, which sends radio waves out and a transponder that receives these radio waves and responds to them by sending radio waves back to the reader. The transponder typically consists of an antenna driven by an integrated circuit, and possibly a power source and radio transmitter depending on the application.

Widespread use of RFID systems did not come about until integrated circuits (ICs) allowed for fabrication of small, low-cost transponders. RFID designers attach these transponders, called tags, to the objects that the transponders identify. The application that has pushed the development of RFID tags the most in the last two decades is the use of RFID tags in supply chain management as a replacement for the barcode. For use in supply chain management, RFID tags need to be inexpensive, small, robust, and they need to have an operating range of at least a few meters. A few other common applications for RFID tags include vehicle identification, animal identification, hospital devices, and passports [1].

Two ways the RFID industry typically classifies RFID systems are by power source and frequency range. The RFID industry classifies systems as passive, active, or semi-passive depending on the power source of the transponder/tag. A passive RFID tag consists of only an antenna and some circuitry, having no independent power source and no radio transmitter. A passive tag backscatters the radio waves from the sender so that they reflect back to the sender as

modulated waves, and also uses the received radio waves as a power source. An active tag has an independent power source, usually a battery, and its own radio transmitter in addition to its antenna and circuitry. A semi-passive tag has its own power source to power its circuitry, but still uses backscattering to respond to the sender [1].

An RFID system can also be classified by the frequency range it uses for its radio communications. The most common frequency bands that RFID systems use are 125/134 kHz, classified as low-frequency (LF); 13.56 MHz, classified as high-frequency (HF); and 860-960 MHz or 2.4-2.45 GHz, classified as ultra-high-frequency (UHF). LF and HF systems typically communicate through inductive coupling, which has a communication distance comparable with the antenna sizes of the sender and receiver. UHF systems communicate with radiative coupling and their communication distances are limited by transmitter power [1]. This thesis focuses on passive UHF RFID tags.

For passive UHF RFID tags, it is common for engineers to design tag antennas that are variations of the T-match antenna [2]. A T-match antenna in its most basic form consists of a simple dipole driven by a T-section feed (see Figure 1 in Chapter 2). T-match antennas are well suited for RFID tags because their inductive T-section feeds can compensate for both the capacitive input impedance of a dipole shorter than resonant length and the capacitive impedance of an IC loading the antenna.

Because of the T-match antenna's common usage by RFID tag engineers, there is benefit in researching ways for designing T-match antennas to operate with wide bandwidths across which they maintain high power transfer efficiency (PTE). Wide bandwidths are useful for worldwide RFID tag operation, as will be discussed in Chapter 3. High power transfer efficiency allows for the range of an RFID system to be maximized with a given input power. Better power

transfer efficiency in a passive RFID tag means less loss between when the tag receives a signal and when it sends a response. More power is then available when an RFID tag responds, allowing for communication over longer distances while still meeting the reader's minimum power requirement. More efficiency in RFID tags could also mean less power needed to communicate over a particular distance, which could in turn lower the cost of RFID readers.

To achieve wide bandwidths with high PTE for small, planar, T-match antennas, different ways of thinking that combine existing RFID tag antenna design theory with other classical Electrical Engineering theory may prove useful. In [2], Deavours addresses UHF RFID design challenges and introduces the concept of designing T-match antennas to behave as band-pass filters in order to maximize bandwidth and other band-pass metrics. Design examples and real-world solutions are provided to show the usefulness of the band-pass model in [2]. This thesis continues from the band-pass model idea presented in [2].

The goal of this thesis is to present a new concept of designing planar T-match antennas to have frequency responses similar to 2nd-order Chebyshev band-pass filters. This concept will then be demonstrated by redesigning an existing commercial RFID tag antenna to have a wider bandwidth with high power transfer efficiency. Chapter 2 begins with two analyses of the T-match antenna that both result in the same basic equivalent circuit form. The analyses are followed by a demonstration that the T-match equivalent circuit form is that of a 2nd-order band-pass filter. Chapter 3 contains the design of a Chebyshev band-pass filter with a frequency response that will be the target for T-match antenna designs. In Chapter 4, an existing commercial UHF RFID tag is introduced that will be redesigned to match the target filter from Chapter 3. In Chapter 5, different antenna geometry features of the commercial antenna from Chapter 4 are revealed that can be tuned to match the antenna's electrical characteristics to those

of the target Chebyshev filter. Chapter 6 shows the simulation results for three antenna designs resulting from using the filter in Chapter 3 as a target for redesigning the commercial antenna in Chapter 4. Chapter 7 concludes this thesis discussing its implications and possible future work.

2. T-match Impedance and Equivalent Circuit

When designing a T-match antenna to have a band-pass filter frequency response, one must establish a theoretical relationship between a T-match and a band-pass filter that will help with comparing the two. Once this relationship has been established, it will be possible to design the elements of the T-match equivalent circuit to match those of a band-pass filter with a desired frequency response. This chapter presents two methods for analyzing a T-match antenna that arrive at the same basic equivalent circuit form. Both methods provide different insights into the behavior of a T-match antenna that will be used later to design antennas with band-pass responses.

The first section of this chapter introduces a T-match analysis method by Uda [3] and the resulting input impedance equation. The next two sections provide more detail about the Uda method and the nature of its input impedance, resulting in a basic equivalent circuit. Sections 4 and 5 elaborate on this equivalent circuit in order to later show that the circuit has the form of a band-pass filter. Section 6 presents a lumped circuit analysis method for analyzing the T-match that arrives at an equivalent circuit with the same form as the one in section 5. Section 7 takes the final step of showing that the T-match equivalent circuit form arrived at in sections 5 and 6 has the form of a band-pass filter.

2.1 Uda's T-match Analysis Method

The first analysis method can be used to demonstrate that the T-match equivalent circuit has the form of a band-pass filter is Uda's analysis method. Uda originally analyzed the T-match antenna in 1954 [3]. The Uda model starts with a basic T-match antenna, as shown in Figure 1.

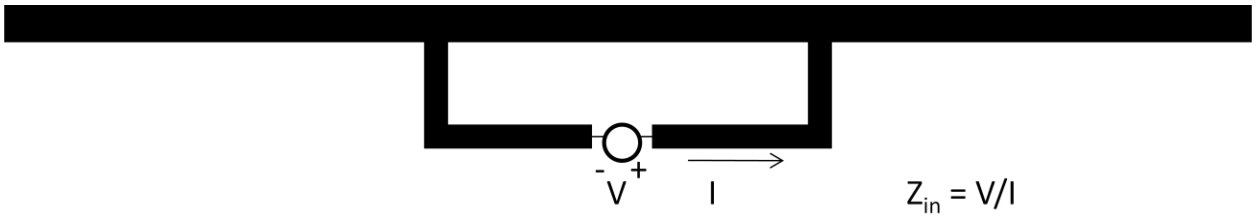

Figure 1: Basic T-match Geometry with Voltage and Current at Driven Port Labeled

The T-match antenna consists of a dipole and a T-section feed with the driven port in the T-section. The antenna has a driven port voltage V and current I, as shown in Figure 1. The Uda model uses the superposition principal to model the antenna, which allows the antenna to be represented in terms of an even-mode response and an odd-mode response. A second, faux, port is added to the antenna structure for this even-/odd-mode analysis. When representing the even-mode or odd-mode of the T-match a source is placed at this second port in order to achieve the even-mode or odd-mode behavior. Figures 2a and 2b represent the even- and odd-mode of the T-match antenna in Figure 1. The response of the T-match antenna will be the sum of its even-mode and odd-mode responses.

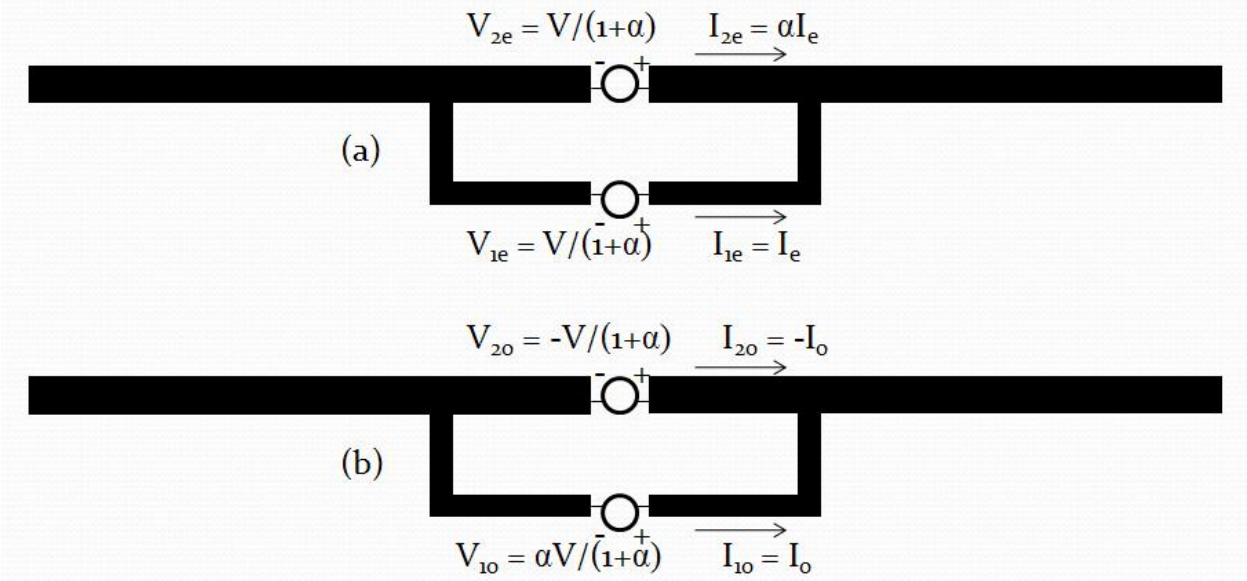

Figure 2: 2-Port Even-Mode (a) and Odd-Mode (b) Representations of the T-match Antenna

The voltages for each mode are chosen so that

$$V_{1e} + V_{1o} = V, \qquad (1)$$

and

$$V_{2e} + V_{2o} = 0, \qquad (2)$$

where V is the driven port voltage for the single-port T-match antenna in Figure 1. The driven port current I in Figure 1 is the sum of the driven port even-mode and odd-mode currents in Figures 2a and 2b, respectively:

$$I = I_{1e} + I_{1o}. \qquad (3)$$

The T-match input impedance is the ratio between the voltage V and the current I at the driven port in Figure 1, and the input admittance is the reciprocal of the input impedance. Using Equation (3), the input admittance is

$$Y_{in} = \frac{I}{V} = \frac{I_{1e}+I_{1o}}{V} = \frac{I_{1e}}{V} + \frac{I_{1o}}{V} = \frac{1}{Z_e} + \frac{1}{Z_o}, \qquad (4)$$

where Z_e is the even-mode impedance and Z_o is the odd-mode impedance. The input admittance is the sum of the even-mode and odd-mode admittances, which are just the reciprocals of the even-mode and odd-mode impedances. From Equation (4), it follows that

$$Z_{in} = \frac{1}{Y_{in}} = \frac{1}{\frac{1}{Z_e}+\frac{1}{Z_o}} = \frac{Z_e Z_o}{Z_e+Z_o} = \frac{(1+\alpha)^2 Z_c Z_o}{(1+\alpha)^2 Z_c+Z_o}, \qquad (5)$$

which shows that the input admittance is the sum of two admittances, and, thus, the input impedance is the parallel combination of the reciprocals of the two summed admittances: Where, Z_c is the common-mode impedance, and α is a splitting factor.

The even-mode impedance Z_e is the ratio between the total driven port voltage V in Figure 1 and the even-mode current I_e in Figure 2a:

$$Z_e = \frac{V}{I_e}. \qquad (6)$$

The odd-mode impedance Z_o is the ratio between the total driven port voltage V in Figure 1 and the odd-mode current I_o in Figure 2b:

$$Z_o = \frac{V}{I_o}. \qquad (7)$$

2.2 Even-Mode Impedance and Splitting Factor

The even-mode represented by Figure 2a has equal voltages driving both ports. This results in port currents that differ by a multiplicative factor of α. The relationship between α and the 2-port z-parameters of the antenna can be derived by starting from the following 2-port z-parameter matrix equation:

$$\begin{bmatrix} V_{1e} \\ V_{1e} \end{bmatrix} = \begin{bmatrix} z_{11} & z_{12} \\ z_{12} & z_{22} \end{bmatrix} \begin{bmatrix} I_{1e} \\ \alpha\, I_{1e} \end{bmatrix}. \qquad (8)$$

Here, V_{1e} has been used for both port voltages since the voltages are equal in the antenna's even-mode. Also, both port currents have been written in terms of I_{1e} so that there are only two unknowns in Equation (8) (not including the z-parameters). Equation (8) can be solved algebraically for the current splitting factor α, resulting in the following equation [4]:

$$\alpha = \frac{z_{11} - z_{12}}{z_{22} - z_{12}}. \qquad (9)$$

The even-mode impedance from Equation (6) can also be written in terms of 2-port z-parameters, starting from one of the two equations within the matrix Equation (8). Choosing the first equation and rearranging it to get V_{1e} divided by I_{1e} gives

$$\frac{V_{1e}}{I_{1e}} = z_{11} + z_{12}\alpha. \qquad (10)$$

Writing V_{1e} in terms of the 1-port voltage V and I_{1e} in terms of I_e gives

$$\frac{V}{(1+\alpha)I_e} = z_{11} + z_{12}\alpha. \qquad (11)$$

After some algebra, the result for Z_e is

$$Z_e = (1 + \alpha)^2 \left[\frac{Z_{11}Z_{22} - Z_{12}^2}{Z_{11} + Z_{22} - 2Z_{12}}\right] = (1 + \alpha)^2 Z_c, \qquad (12)$$

where the term in square brackets in Equation (12) is the 2-port z-parameter form of the common-mode impedance Z_c.

The common-mode impedance Z_c is the impedance that a single source sees when the T-match is driven in the even-mode and the source is connected to both ports in parallel. Figure 3 represents the T-match antenna in the common-mode.

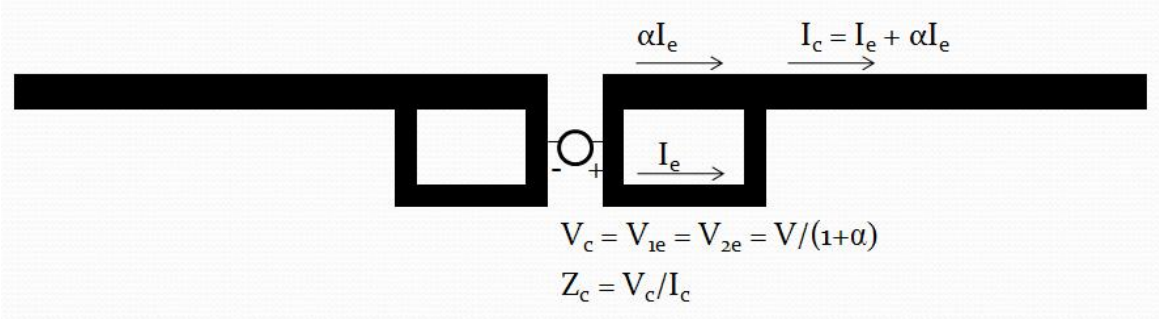

Figure 3: T-match Common-Mode Illustration

Z_c is the ratio between the common-mode voltage V_c and the common-mode current I_c. The common-mode voltage is the same as the voltage across both ports in the even-mode V_{1e}. The common-mode current is the sum of the currents across both ports of the even-mode, I_e and αI_e. Using this information, the common-mode impedance is

$$Z_c = \frac{V_c}{I_c} = \frac{V_{1e}}{(1+\alpha)I_e} = \frac{V}{(1+\alpha)^2 I_e} = \frac{Z_e}{(1+\alpha)^2}. \qquad (13)$$

The final result in Equation (13) is just a rearranged version of Equation (12). Now that Z_e and Z_c are in terms of 2-port z-parameters, the odd-mode impedance is next.

2.3 Odd-Mode Impedance and Splitting Factor

The odd-mode represented by Figure 2b has currents that are equal in amplitude but opposite in phase. The odd-mode also has voltages that differ by a multiplicative factor of $-\alpha$. The voltage splitting factor can be derived starting from the following 2-port z-parameter matrix equation:

$$\begin{bmatrix} -\alpha V_{2o} \\ V_{2o} \end{bmatrix} = \begin{bmatrix} z_{11} & z_{12} \\ z_{12} & z_{22} \end{bmatrix} \begin{bmatrix} -I_{2o} \\ I_{2o} \end{bmatrix}. \qquad (14)$$

Here, both port voltages have been written in terms of V_{2o} and both port currents have been written in terms of I_{2o} so that there are only two unknowns (not including the z-parameters). Equation (14) can be solved algebraically for the voltage splitting factor α, resulting in the following equation [4]:

$$\alpha = \frac{Z_{11} - Z_{12}}{Z_{22} - Z_{12}}. \qquad (15)$$

Equations (9) and (15) are identical, showing that the splitting factors for the even-mode and odd-mode are the same.

The odd-mode impedance can be written in terms of 2-port z-parameters by starting from one of the two equations within the matrix Equation (14). Choosing the second equation and rearranging it to get V_{2o} divided by I_{2o} gives

$$\frac{V_{2o}}{I_{2o}} = z_{22} - z_{12}. \qquad (16)$$

Writing V_{2o} in terms of the 1-port voltage V and I_{2o} in terms of I_o gives

$$\frac{-V}{-(1+\alpha)I_o} = z_{22} - z_{12}. \qquad (17)$$

After some algebra and substituting for α using Equation (15), the result for Z_o is

$$Z_o = Z_{11} + Z_{22} - 2Z_{12}. \qquad (18)$$

Figures 4 and 5 depict two different, yet equivalent circuits that represent the input impedance of the T-match. The circuit in Figure 4 represents the input impedance in terms of the even-mode and odd-mode impedances whereas the circuit in Figure 5 represents the input

impedance in terms of the odd-mode impedance, the common-mode impedance, and the splitting factor α.

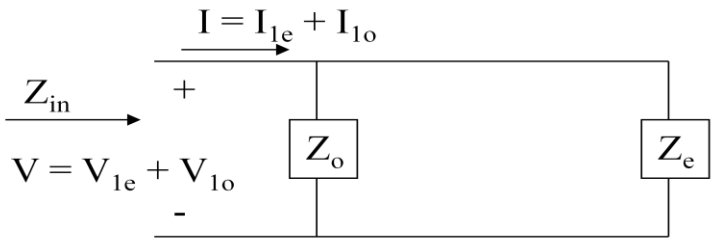

Figure 4: Equivalent Circuit for T-match Antenna Impedance in Terms of Z_e and Z_o

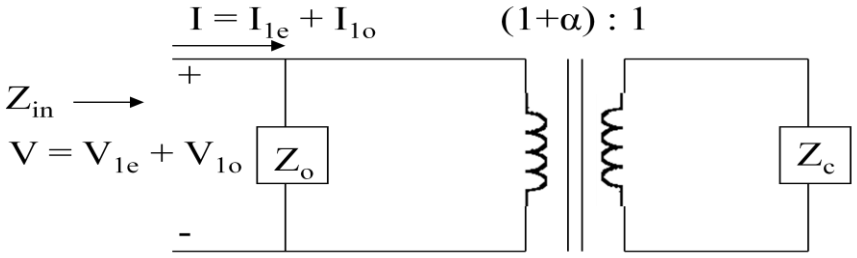

Figure 5: T-match Equivalent Circuit in Terms of Z_o, Z_c, and α

In Figure 5, the transformer replaces the factor of $(1+\alpha)^2$ in Equation (12) that transforms Z_c into Z_e. Both equivalent circuits are useful for understanding how the T-match antenna input impedance behaves, but it is not apparent just from these circuits that the T-match can have the form of a band-pass filter.

2.4 Common-Mode Impedance Equivalent Circuit

This section develops an equivalent circuit form for Z_c based on the geometry of the T-match common-mode in Figure 3, which is essentially a non-uniform dipole. Finding an equivalent circuit for Z_c will help in demonstrating that the T-match equivalent circuit can have the form of a band-pass filter. One can approximate the common-mode non-uniform dipole's port impedance with the impedance of a uniform dipole. The uniform dipole that Uda used for this approximation has a radius that is a function of the radii of the two T-match conductors and the spacing between them [3]. A similar approximation can be made for a T-match with planar conductors.

Approximating the common-mode impedance as that of a uniform dipole helps simplify the T-match impedance analysis, but the form of this common-mode impedance is still needed. In [5], Hamid and Hamid developed an equivalent circuit that approximates the form of the input impedance of a dipole near its first few resonances. The equivalent circuit from [5] is in Figure 6b. The frequency response of the dipole equivalent circuit from [5] is illustrated by the plot in Figure 6a. The solid line on the graph represents the real part of the input impedance of the dipole equivalent circuit while the dashed lines represent the imaginary part of the input impedance. The reactive contributions to the dipole impedance give a first resonance of the dipole approximately halfway between the zero frequency point (left edge of the graph) and the second resonance, which is at the zero-crossing of X_1.

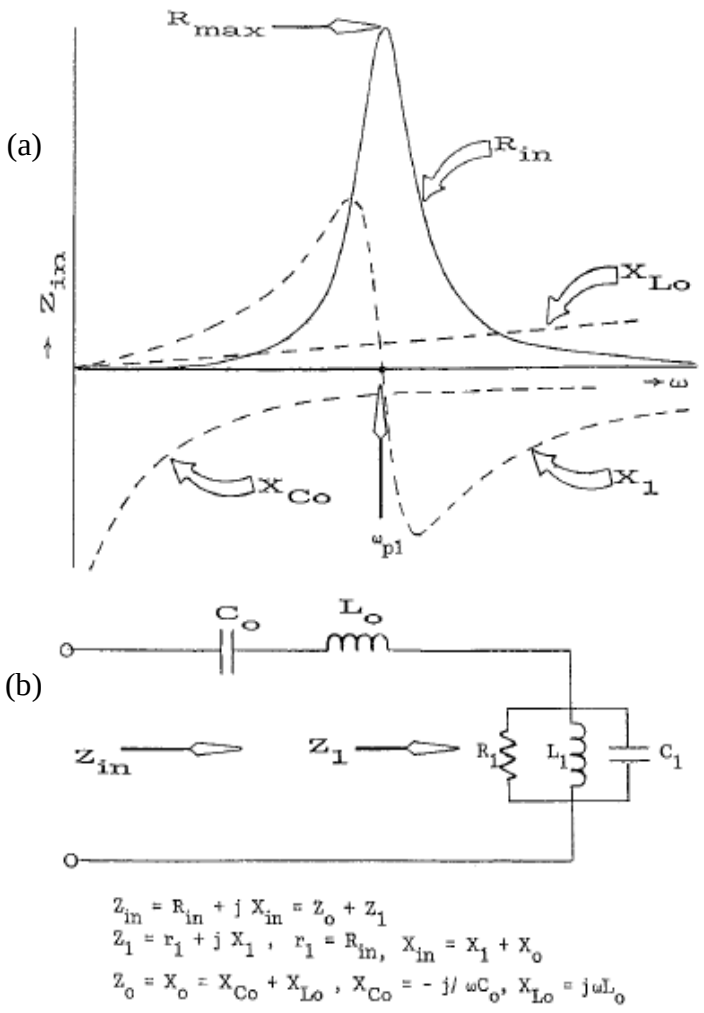

Figure 6: Dipole Impedance Plot (a) and Equivalent Circuit (b) from [5]

To have an antenna with a band-pass frequency response, the common-mode impedance of the T-match will be operated near the first resonance point. One can simplify the dipole equivalent circuit given in Figure 6b when the impedance operation is restricted to near the first resonance. The graph in Figure 6a shows that the main contribution of the reactance X_1 around the first resonance is inductance, and this inductance is a fairly linear function of frequency. The shunt inductor L_1 and the shunt capacitor C_1 can be removed from the circuit in Figure 6b and

instead the value of the series inductor L_o can be increased to approximate the same effect on the reactance. This simplifies the dipole equivalent circuit to a series RLC circuit.

2.5 Odd-Mode Impedance Equivalent Circuit

Uda modeled the odd-mode impedance Z_o by making the assumption that the odd-mode is a TE mode associated with a transmission line [3]. In the odd-mode, this TE mode assumption ignores the dipole part of the antenna geometry and the T-match is driven as a loop. Figure 7 shows the odd-mode of the T-match without dipole arms.

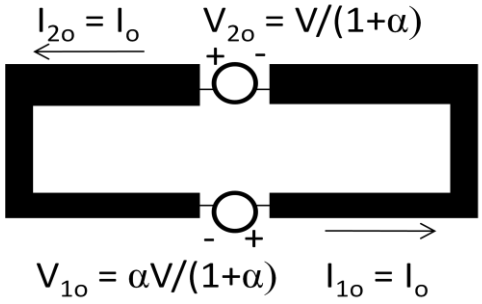

Figure 7: T-match Odd-Mode without Dipole Arms

According to Equation (7), the odd-mode impedance Z_o is the ratio between the single-port voltage V and the odd-mode inductance I_o. Z_o is also equivalent to the ratio between the total voltage and the total current around the loop in Figure 7:

$$\frac{V_{1o}+V_{2o}}{I_o} = \frac{(1+\alpha)V}{(1+\alpha)I_o} = \frac{V}{I_o} = Z_o. \qquad (19)$$

The nature of Z_o can be found from viewing the two halves of the odd-mode loop in Figure 7 as short-circuited transmission lines. This is accomplished by dividing the odd-mode loop in half at its zero-potential line as shown in Figure 8.

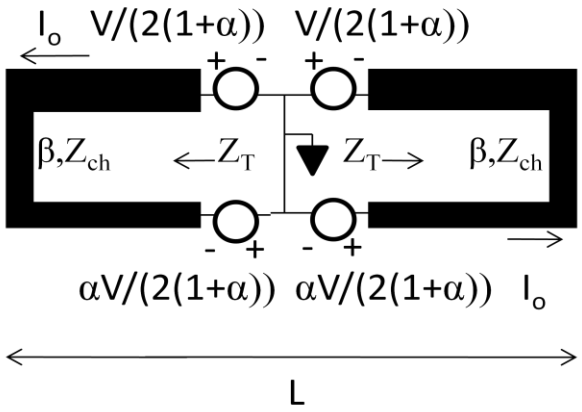

Figure 8: T-match Odd-Mode Divided at Zero-Potential Line

In the figure, a line connected to ground represents the zero-potential line dividing the odd-mode loop. The sources have each been divided into two sources with half the voltage of the original source, one on either side of the zero-potential line. The impedances Z_T in this figure represent the transmission line input impedances looking into each half of the T-section feed loop from the center. Both transmission lines have the same characteristic impedance Z_{ch} and the same propagation constant β. The potential across each transmission line is the sum of the two voltage sources on the respective half of the zero-potential line. Dividing the voltage across one of the transmission lines by the current through that transmission line gives the transmission line impedance Z_T:

$$Z_T = \frac{(1+\alpha)V}{2(1+\alpha)I_o} = \frac{V}{2I_o} = \frac{Z_o}{2}. \qquad (20)$$

Since Z_T is the input impedance of a short-circuited transmission line, it can also be written as

$$Z_T = jZ_{ch}\tan\left(\frac{\beta L}{2}\right), \qquad (21)$$

where Z_{ch} is the characteristic impedance of the transmission lines, β is the phase constant of the transmission lines, and L is the length of the T-section feed. Combining Equations (20) and (21), the odd-mode impedance becomes

$$Z_o = 2Z_T = j2Z_{ch}\tan\left(\frac{\beta L}{2}\right). \qquad (22)$$

Equation (22) shows that the odd-mode impedance is purely reactive. Also, since the transmission lines are relatively short compared to the T-match length and, hence, the operating wavelength, the odd-mode impedance is typically inductive. The validity of Uda's transmission line assumption for planar T-match antennas has been verified in [6].

Figure 9 displays the T-match equivalent circuit with an inductor representing Z_o and series RLC components representing Z_c.

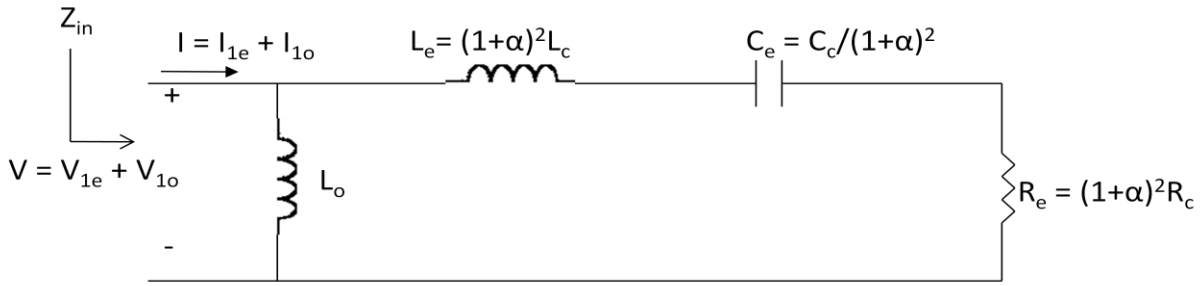

Figure 9: T-match Antenna Impedance Equivalent Circuit

The equivalent circuit in Figure 9 has some elements of a band-pass filter, but by itself is still missing some pieces. A series resonant pair is present with L_e and C_e, and R_e could be either a source or load resistance. If a shunt capacitor and resistor pair is connected to the circuit terminals at the left, than the circuit would be a 2nd-order band-pass filter with source and load resistances. Loading the antenna with an integrated circuit (IC) could solve the problem of an incomplete filter, but first a lumped circuit analysis method for analyzing the T-match antenna will be presented.

2.6 Lumped Circuit Analysis Method

The second T-match analysis method is a lumped circuit approximation that results in an equivalent circuit similar to the one in Figure 9. Each of the conductors in the T-match geometry has some capacitance and inductance associated with it. When using a planar T-match antenna, the capacitance will be minimal since the conductor surfaces facing each other are very thin. With minimal capacitance from coupling for a planar T-match, it simplifies the analysis to neglect this capacitance completely. The inductive coupling between conductors cannot simply be neglected in this way. However, according to [2], treating the short T-section feed traces as lumped inductors without coupling will result in a qualitatively correct equivalent circuit for the T-match.

First, consider the two main parts of the T-match in Figure 10, the dipole section and the T-section feed loop.

Figure 10: T-match Dipole Section and T-section Feed Loop

In the figure, the dipole and T-section feed loop are separated, and terminals are shown to represent where the two parts would be connected when the T-match is whole. The impedance across the dipole terminals can be approximated near its first resonance by a series RLC circuit as was discussed in Section 2.4. The dipole in Figure 10 appears to have a rather wide feed gap. This is partly due to exaggeration of the size of the T-section feed for illustrative purposes. In practice, variations of the T-match are used that have relatively small feed gap widths, so there

should be no issue with too wide of a dipole feed gap. If a dipole with too wide of a feed gap is used, a more complex input impedance approximation may be needed.

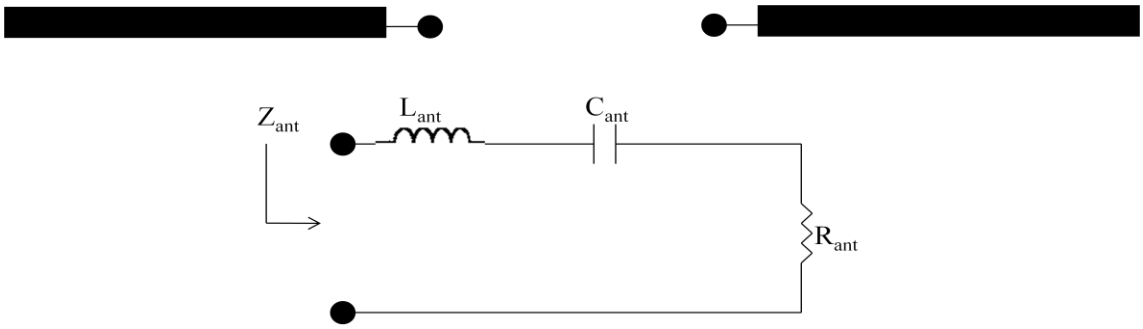

Figure 11: T-match Dipole Section and Equivalent Circuit.

Figure 11 shows the RLC approximation for the impedance measured across the terminals of the dipole part of the T-match. The terminals of the dipole equivalent circuit, represented by large dots, correspond to the terminals of the dipole structure above the circuit.

Using the assumption that the T-section feed conductors can be treated as lumped inductances, one can model the traces of the T-section feed loop as inductances.

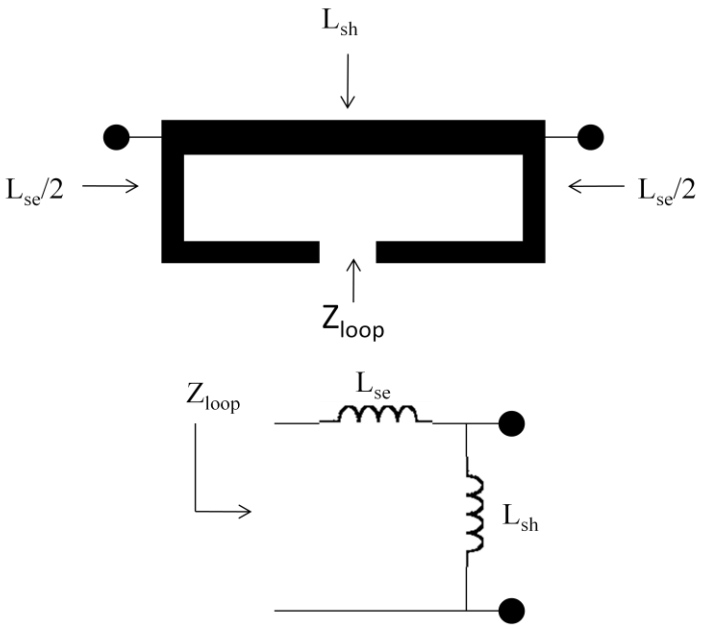

Figure 12: T-match Feed Loop and Equivalent Circuit

In Figure 12, L_{se} is the inductance for the sides and bottom of the T-section feed loop and L_{sh} is the inductance for the top section of the loop that sits between the terminals where the dipole would be connected.

Putting the two T-match impedance components in one circuit in Figure 13, L_{sh} is an inductor between the dipole terminals and L_{se} is an inductor in series with the dipole terminals.

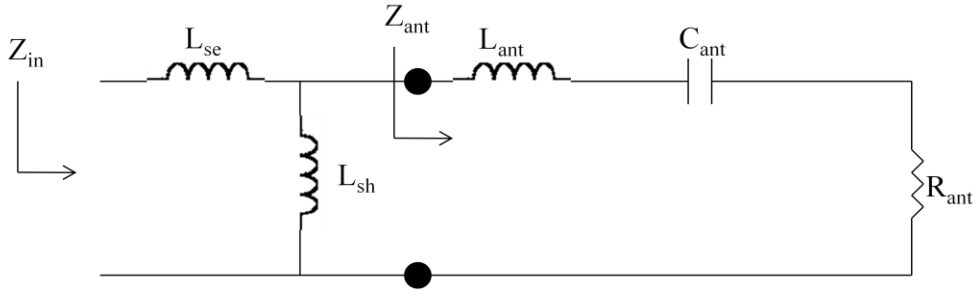

Figure 13: T-match Impedance Equivalent Circuit from Lumped Circuit Approximation

The circuit in Figure 13 looks similar to the equivalent circuit from the previous section (Figure 9), but there are two major differences. The circuit in Figure 13 has an inductor in series that is not present in Figure 9, and in Figure 13, the RLC dipole impedance components do not have the scaling factor $(1+\alpha)^2$. These two differences can be partially resolved by a transformation similar to the one presented in [2]. The transformation uses a scaling factor β that is a function of L_{se} and L_{sh}:

$$\beta = \frac{L_{se}+L_{sh}}{L_{sh}}. \qquad (23)$$

The scaling factor β is the total T-section feed loop inductance divided by the T-section feed loop inductance that is part of the dipole. Equations (24) through (28) map the original circuit components from Figure 13 to transformed circuit components:

$$R'_{ant} = \beta^2 R_{ant} \qquad (24)$$

$$L'_{ant} = \beta^2 L_{ant} \qquad (25)$$

$$C'_{ant} = \frac{C_{ant}}{\beta^2} \qquad (26)$$

$$L'_{se} = \beta L_{se} \qquad (27)$$

$$L'_{sh} = \beta L_{sh} \qquad (28)$$

Figure 14 shows the T-match equivalent circuit composed of the transformed circuit components.

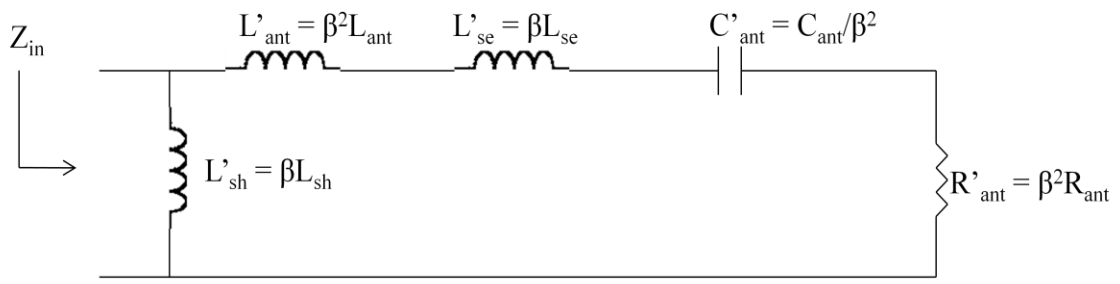

Figure 14: Transformed T-match Impedance Equivalent Circuit from Lumped Circuit Approximation

The circuit in Figure 14 can be simplified by combining the two series inductors, L'_{se} and L'_{ant}, as shown in Figure 15.

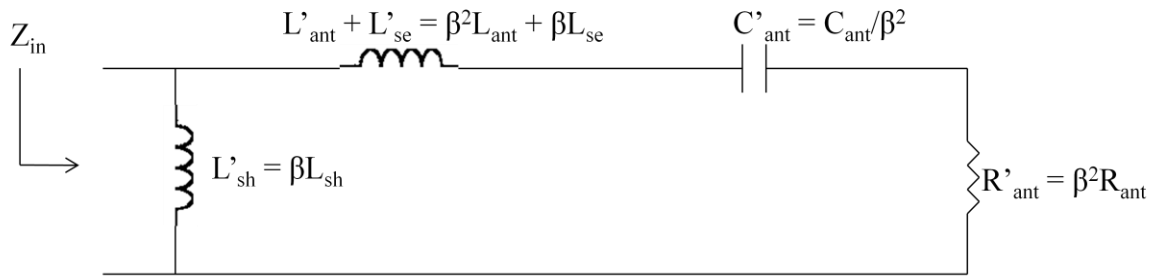

Figure 15: Transformed T-match Impedance Equivalent Circuit from Lumped Circuit Approximation with Combined Series Inductors

The circuit in Figure 15 is very similar to the circuit in Figure 9. The scaling factor β here is comparable to the factor of (1+α) from Figure 9, but they are not exactly the same. For example, β scales the shunt inductance in this circuit, but (1+α) does not scale the shunt inductance in Figure 9. The RLC antenna impedance components from this lumped circuit approximation are not quite equivalent to the common-mode impedance components in the previous section. The common-mode impedance approximates a non-uniform dipole by treating it as a uniform dipole with an effective radius/width, while the dipole impedance approximation in this section's

analysis uses the antenna's original radius/width. Another major difference between the circuit in Figure 15 and the one in Figure 9 is that the circuit in Figure 15 has extra inductance added to the series inductance. Despite the differences between the circuits in Figure 15 and Figure 9, both circuits do have the same basic form of an inductance in parallel with a series RLC impedance.

2.7 T-match Antenna as a Band-Pass Filter

Now that it has been established established that the input impedance of a T-match antenna can have the form of an inductor in parallel with a series RLC impedance, it will now be demonstrated that this form is that of a band-pass filter when an appropriate load is attached. When one uses a T-match antenna as a passive UHF RFID antenna, the antenna has an IC connected at its port and can be viewed as a receiver. In this case, the antenna itself becomes the source in the equivalent circuit, and its load is the equivalent circuit of the IC attached at its port. The basic equivalent circuit for a receiving antenna from [7] is in Figure 16.

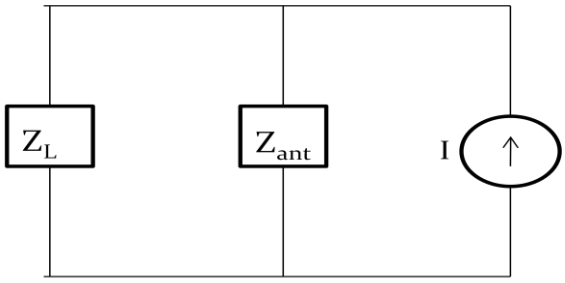

Figure 16: Receiving Antenna Equivalent Circuit in Norton Equivalent Form

Here, Z_{ant} is the input impedance of the antenna, the current source represents the signal being received by the antenna, and Z_L is a load attached to the antenna terminals. If the T-match input impedance circuit from Figure 9 is placed into the Norton equivalent form in Figure 16, and a shunt RC circuit is used as the load equivalent circuit of an IC attached to the T-match port, then the T-match antenna equivalent circuit becomes the circuit shown in Figure 17.

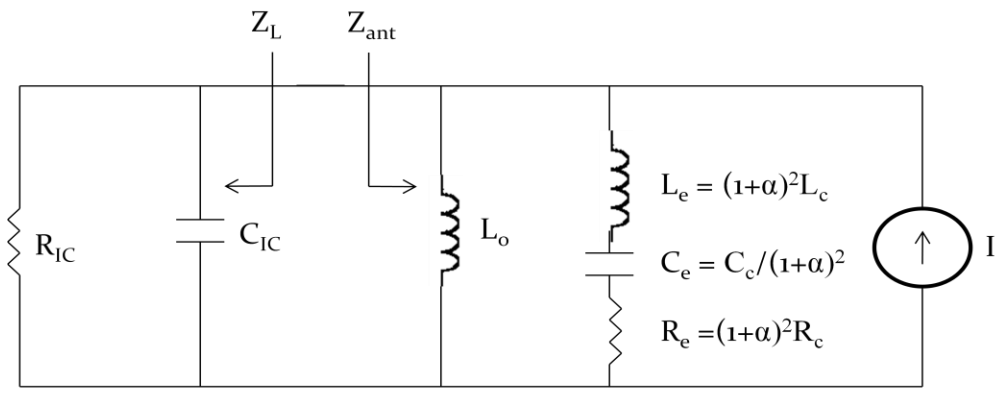

Figure 17: T-match Equivalent Circuit Including IC Impedance (Left Resistor and Capacitor) and Current Source

The port of the T-match antenna in the figure is located at the arrow pointing from Z_{ant}. The components to the left of this point represent typical input impedance components of an IC that would load a passive UHF RFID T-match antenna. The source at the right of the circuit represents the current produced from the antenna receiving a signal.

To simplify this equivalent circuit into a form recognizable as a band-pass filter, a Norton-to-Thevenin transformation is used for all of the circuit components to the right of the odd-mode inductor (not including the odd-mode inductor). The transformation changes the shunt RLC components on the right into series RLC components and changes the current source to a voltage source, producing the circuit shown in Figure 18.

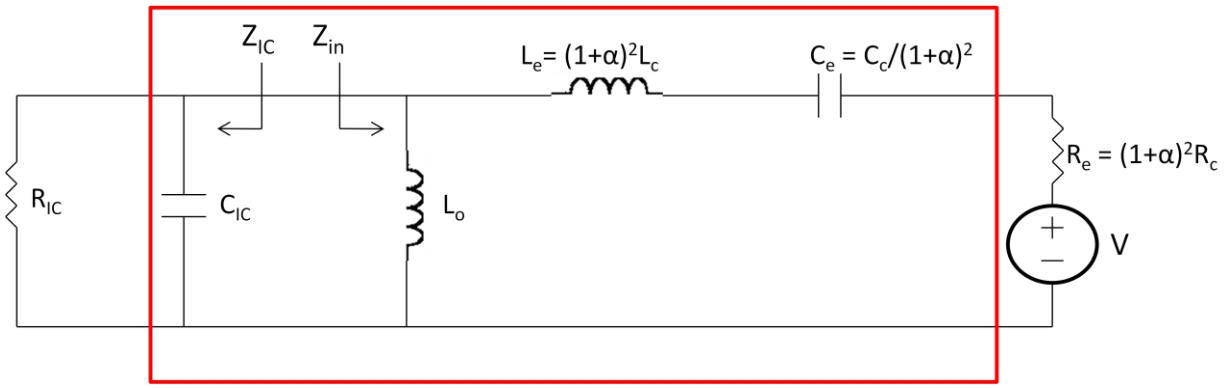

Figure 18: T-match Equivalent Circuit with Source and IC Impedance after Norton-to-Thevenin Transformation

With the circuit form in Figure 18, the inductor/capacitor pairs in the center of the circuit (in the box) have the form of a 2nd-order band-pass filter. Knowing this, these circuit components just need to be designed to produce a useful filter-like response for the T-match antenna. In the next chapter, a filter will be designed with a frequency response desired for a T-match antenna. The filter elements will provide target values that the T-match circuit elements can be designed to match.

3. A Lumped Prototype Filter Design and Characteristics

The first step in designing a T-match antenna that has a band-pass frequency response is to design a lumped prototype band-pass filter with the desired frequency response of a broadband T-match antenna. This filter's frequency response and lumped element values will be used as targets for designing an antenna with an appropriate integrated circuit (IC) for a load. The design of this target filter begins with choosing the desired pass-band characteristics: the pass-band frequency range and whether the pass-band is maximally flat, rippled, or constant phase among other characteristics. Once the pass-band characteristics are chosen, the target filter can be designed.

In this chapter, a target filter is designed that has a frequency range encompassing known world-wide UHF RFID tag frequencies. Section one reveals these frequencies and the filter type chosen. Sections two, three, and four demonstrate the design of a target filter that meets the frequency requirements in section one. In section five, electrical characteristics are revealed that can be used to describe the behavior of the target filter (or T-match antenna). Section six ends the chapter with a discussion of the metric used in this thesis to measure filter/antenna frequency response, which is power transfer efficiency.

3.1 Frequency Requirements and Filter Type

The pass-band characteristics that will be chosen to design the target filter depend on the application in which the T-match antenna will be used. Since this thesis is focusing on the use of T-match antennas in UHF RFID tags, it is appropriate to choose a desired frequency range that includes the frequencies for world-wide UHF RFID tag operation.

Different countries allow different frequency bands to be used for UHF RFID tags, which results in a wide range of frequencies (from 864 MHz to 954 MHz) as shown in Figure 19 [1]. The 860-960 MHz region is regulated differently by the governments of different countries to try and manage RFID, cell phones, and many other applications that would like to use these frequencies.

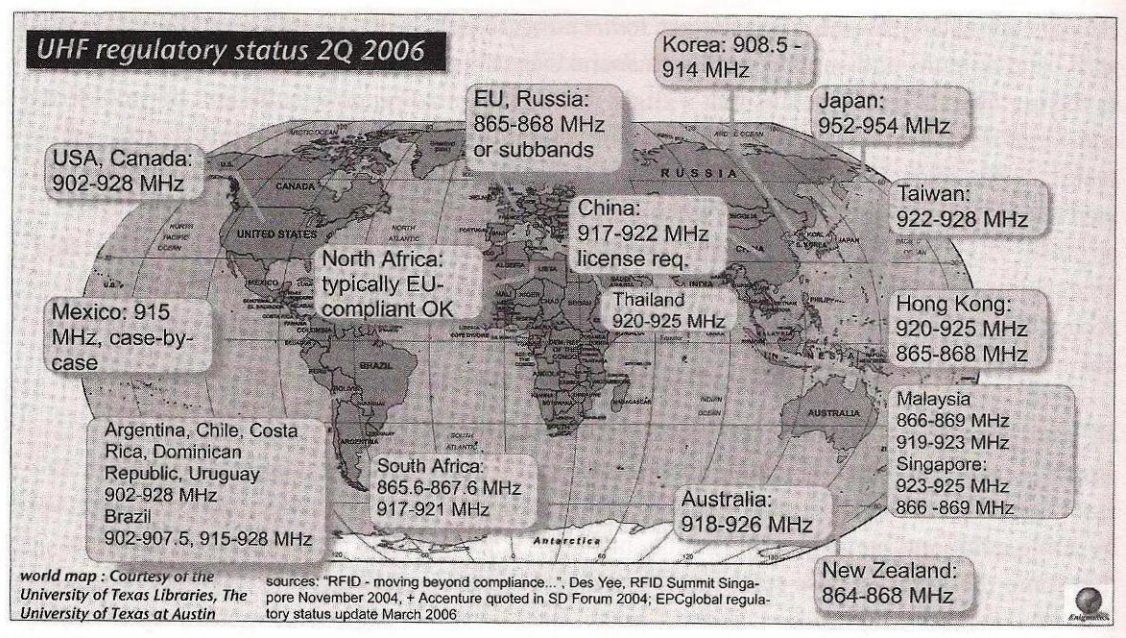

Figure 19: World-Wide RFID Frequency Bands from [1]

To keep the filter design simple, a good choice for the type of filter is a Chebyshev filter. Maximally flat filters are also simple to design, but a Chebyshev filter offers a wider bandwidth for a lower order filter. Chebyshev filters also offer a steeper transition region which allows for better rejection of frequencies just outside the pass-band. A Chebyshev filter has ripples in the pass-band of the filter while a maximally flat filter would not. For a simple RFID tag antenna response, ripple in the pass-band is acceptable. Ripple in the pass-band means that the

magnitude of the signal returned by an RFID tag varies in amplitude across its bandwidth. This could be problematic if RFID tags used complex amplitude and frequency modulation, but typically RFID systems use coded on-off keying and/or simple phase modulation to keep the passive tags' signal processing to a minimum. An elliptical filter would provide an even steeper transition region than a Chebyshev filter and also has ripples both in the stop-band and the pass-band, but the Chebyshev transition region is sufficient for RFID tags, and ripples in the stop band are relatively unimportant to simple RFID tags. If linear phase had been needed, then a Bessel filter could have been used, but linearity of phase is not of primary concern in RFID tags.

3.2 Low-Pass Filter Prototype

Lumped element Chebyshev band-pass filters can be designed using well-developed procedures found in texts such as [8] or [9]. The first step in the prototype filter design in [9] begins with a normalized low-pass filter that will later be transformed into a band-pass filter. RFID antennas require low loss within the pass-band, so a ripple maximum of 0.5 dB was chosen. The bandwidth chosen in the previous section was 864-954 MHz, a bandwidth of 90 MHz, but the bandwidth does not come into the design process until the next section. In [9], there is a table of element values provided that gives the normalized low-pass prototype filter lumped element values. These normalized element values come from using the insertion loss method and solving a power loss ratio equation for the desired filter order and type. Figure 20 shows the low-pass filter prototype with normalized element values taken from the table in [9].

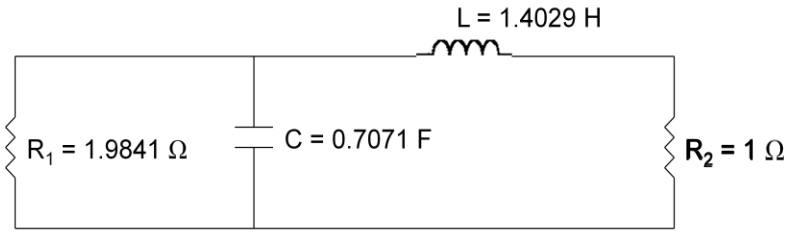

Figure 20: Normalized Low-Pass Filter Prototype with Normalized Element Values [9]

3.3 Transformation to Band-Pass Filter

The second step in the Chebyshev design procedure in [9] is to transform the normalized low-pass prototype into a normalized band-pass filter. To accomplish this, a bandwidth parameter Δ is needed that is the ratio between the chosen bandwidth and the center frequency. The equation for Δ is

$$\Delta = \frac{\omega_2 - \omega_1}{\omega_0}, \qquad (29)$$

where ω_2 is the upper cutoff frequency of the desired pass-band, ω_1 is the lower cutoff frequency of the desired pass-band, and ω_0 is the center frequency of the desired pass-band. The pass-band chosen here is 864-954 MHz for worldwide UHF RFID tag operation. This means that ω_2 is 2π x 954 rad/s and ω_1 is 2π x 864 rad/s. The center frequency for this frequency band can be found from the geometric mean of the upper and lower cutoff frequencies:

$$\omega_0 = \sqrt{\omega_1 * \omega_2}. \qquad (30)$$

Using Equation (30) gives a center frequency of 2π x 908 rad/s. With the center and cutoff frequencies known, Δ can be calculated from Equation (29) to be approximately 0.099.

Now the normalized low-pass filter can be transformed into a normalized band-pass filter. This transformation is performed using the following equations from [9] that transform L and C each into a capacitor and inductor pair:

$$L_s = \frac{L}{\Delta * \omega_0} \qquad (31)$$

$$C_s = \frac{\Delta}{L * \omega_0} \qquad (32)$$

$$C_p = \frac{C}{\Delta * \omega_0} \qquad (33)$$

$$L_p = \frac{\Delta}{C * \omega_0} \qquad (34)$$

Calculating the values for the four elements from Equations (31)-(34) gives the values shown in Figure 21.

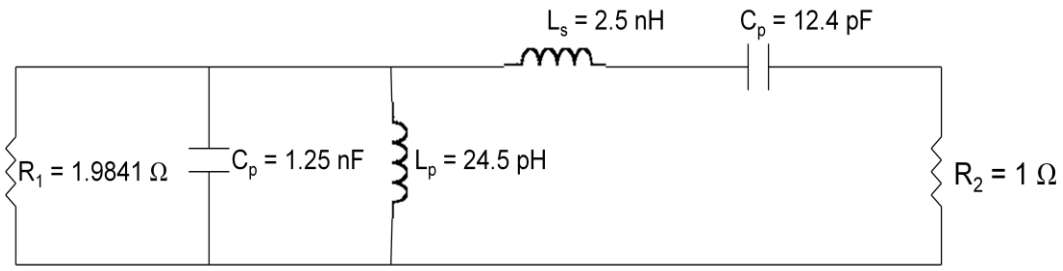

Figure 21: Frequency-Scaled Band-Pass Filter Prototype

3.4 De-normalizing the Filter

The final step in the Chebyshev design procedure in [9] is to de-normalize the normalized band-pass filter by scaling its components by the appropriate resistance. From Figure 21, R_1 is the IC resistance from the circuit in Figure 18 and R_2 is the radiation resistance, or even-mode resistance. The IC resistance will be easier to set to a desired value without altering the antenna itself. Setting the IC resistance is as simple as choosing an appropriate IC to load the antenna, but resistance is not the only concern when choosing an IC.

An IC with the same Q as the normalized band-pass filter needs to be chosen. From the frequency-scaled circuit in Figure 21, the Q value for the parallel RLC section can be calculated by

$$Q_p = R_1 * C_p * \omega_0. \qquad (35)$$

The Q value calculated from Equation (35) is approximately 14.2. This Q value will not change after the circuit is scaled for resistance because the scaling will multiply R_1 and C_p by reciprocal values.

There are many ICs available commercially. Table 1 shows a number of ICs that RFID manufacturers have produced in the last decade, along with their impedances and Qs. The table is not an exhaustive list of all ICs. Rather, it is meant to provide some examples and show the variety and range of impedances and Q values available from commercial ICs that were designed for RFID tags. The impedances listed in the table are the equivalent impedances when viewing the IC's impedance as a shunt resistor/capacitor pair.

Table 1: Example ICs Commercially Available in the Last Decade

IC Name [source]	Resistance (Ω)	Capacitance (pF)	Q
Monza [10]	415	1.4	3.4
Monaco64 [11]	389	1.9	4.2
Higgs-3 [12]	1500	0.85	7.3
Monza 3 [13]	1350	1.2	9.2
Higgs-2 [14]	1500	1.2	10.3
Monza 4 [15]	1000	2.48	14.3
EM4324 [16]	4200	0.88	21.2
XRAG2 [17]	6012	0.71	24.5
XRA00 [18]	5800	0.88	29.3

From the examples in Table 1, the IC with Q value closest to 14.2 is the Monza 4 IC with a shunt resistance of 1000 Ω and a shunt capacitance of 2.48 pF. This IC will be used throughout the rest of the design process. If the decision is made later to change ICs, then the target filter will have to be redesigned starting at this point, using the new IC impedance.

The Monza 4 IC's impedance provides a value for R_1 of 1000 Ω. Dividing R_1 by 1.9841 gives the value for R_2 of about 504 Ω. According to [9], to scale the rest of the circuit elements to these resistances, the capacitances in Figure 21 are divided by R_2 and the inductances in Figure 21 are multiplied by R_2. This results in the final filter circuit in Figure 22.

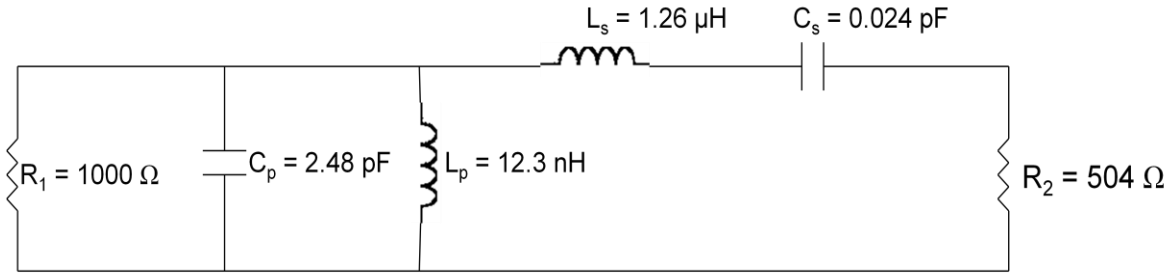

Figure 22: Final Target Band-Pass Filter (without Voltage Source)

3.5 Electrical Characteristics for Antenna Design

This section introduces four electrical characteristics that must be managed when designing a T-match antenna to match the target filter. One way to accomplish this would be to simply use the filter elements in Figure 22 as targets for the impedance elements of the T-match equivalent circuit. However, instead of trying to match an antenna's behavior to individual circuit elements, it is easier to translate some of the circuit elements from Figure 22 (and Figure 18, the T-match equivalent circuit) into electrical characteristics that better represent the circuit's behavior and are simpler to find from simulation results. Assuming that the IC resistance and capacitance are relatively constant with frequency, the other four circuit elements can be translated into four electrical characteristics to focus on when designing a T-match antenna to have the frequency response of the target filter.

The first of these electrical characteristics is the even-mode resistance R_e. This characteristic is simply one of the circuit elements from the T-match equivalent circuit. Dividing the T-match equivalent circuit into a series half and a shunt half, the even-mode resistance completely describes the real part of the series half of the circuit's impedance. Therefore, the real part of the even-mode impedance is a good characteristic to focus on when designing a T-match to match a target filter. In the prototype filter represented by Figure 22, the even-mode resistance is the series resistance R_2, so no further calculation is needed. How to find this characteristic from simulation results will be discussed in Chapter 4.

The series resonant frequency is the next of the four electrical characteristics to focus on when designing a T-match antenna to match a target filter. For the target filter circuit in Figure 22, the series resonant frequency was calculated using Equation (30) and is 908 MHz. This frequency can also be calculated using the circuit element values and Equation (36):

$$\omega_0 = \frac{1}{\sqrt{L_e C_e}}. \qquad (36)$$

where L_s and C_s in Figure 22 are the even-mode inductance, L_e and the even-mode capacitance, C_e, respectively. From antenna simulation results, the series resonant frequency is simply the zero-crossing frequency of the even-mode reactance.

The series (even-mode) Q is the third electrical characteristic that should be observed. Finding this characteristic does require finding one of the two series reactive components, but not both, so it is still simpler than finding all the individual circuit elements. For instance, if the series resonant frequency and even-mode resistance are already known, then the even-mode inductance is the only other component needed to find the series Q:

$$Q_e = \frac{\omega_0 * L_e}{R_e}. \qquad (37)$$

The series Q of the target filter in Figure 22 can be calculated by plugging in L_s for L_e, R_2 for R_e, and 908 MHz * 2π for ω_0 in Equation (37), resulting in a Q of 14.2. How to find the even-mode inductance from simulation results will be discussed in Chapter 4.

The final electrical characteristic to focus on is the odd-mode inductance. This characteristic is simply the imaginary part of the odd-mode impedance. The odd-mode inductance of the target filter in Figure 22 is L_p, which is 12.3 nH. This inductance can be found directly from the Z-parameters of the T-match antenna, which will be discussed in Chapter 4.

The values of the four electrical characteristics described above for the target filter circuit can be found using the circuit element values in Figure 22 and the descriptions of the characteristics in this section. Table 2 shows the target filter electrical characteristic values.

Table 2: Electrical Characteristics for Target Band-Pass Filter

Electrical Characteristic	Target Filter Value
Even-Mode Resistance	504 Ω
Series Resonant Frequency	908 MHz
Series Q	14.2
Odd-Mode Inductance	12.3 nH

These four electrical characteristics completely describe the impedance behavior of the antenna portion of the T-match equivalent circuit. It is also arguably simpler to find the series resonant frequency and series Q from simulation results than to find both the even-mode inductance and capacitance. Therefore, these four electrical characteristics should be the focus when designing a T-match antenna to have a frequency response that matches the response of the target filter.

3.6 Power Transfer Efficiency

In this thesis, the metric used to characterize frequency response is power transfer efficiency. Power transfer efficiency is not to be confused with sensitivity, a more common metric that is often shown on RFID tag specification sheets. Sensitivity is a measure of the minimum input power required for a device to be able to operate how it was intended. The power transfer efficiency is the power transferred to the load of a circuit divided by the maximum power available to the load. The circuit shown in Figure 23 helps illustrate this concept.

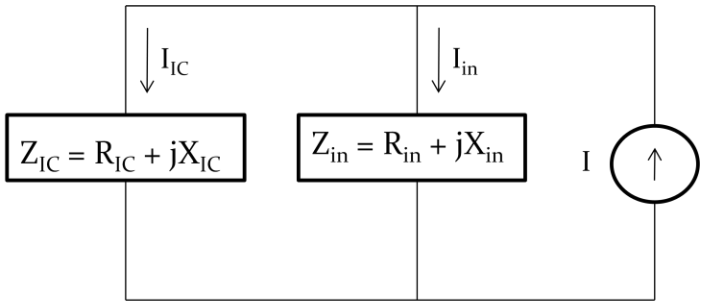

Figure 23: Circuit with Current Source, T-match Input Impedance Z_{in}, and IC Impedance

The circuit in Figure 23 is a more general form of the circuit in Figure 17. In this circuit, Z_{in} is the input impedance to the T-match antenna and is the source impedance. Z_{IC} is the input impedance of the IC attached to the T-match port and is the load impedance. The power transferred to the load is found from multiplying half the square of the magnitude of the current through the load by the real part of the load impedance R_{IC}:

$$P_L = \frac{1}{2}|I_{IC}|^2 R_{IC} = \frac{1}{2}\frac{|I|^2|Z_{in}|^2 R_{IC}}{|Z_{in}+Z_{IC}|^2}. \qquad (38)$$

where P_L is the power transferred to the load.

The maximum power available to the load for the circuit in Figure 23 occurs when maximum power transfer occurs, when Z_{in} and Z_{IC} are complex conjugates. The maximum power available to the load is found from multiplying half the square of the magnitude of the current through the source impedance by the real part of the source impedance R_{in}:

$$P_M = \frac{1}{2}|I_{in}|^2 R_{in} = \frac{1}{2}\frac{|I|^2|Z_{IC}|^2 R_{in}}{|Z_{in}+Z_{IC}|^2} = \frac{1}{2}\frac{|I|^2|Z_{IC}|^2 R_{in}}{|2R_{in}|^2} = \frac{|I|^2|Z_{IC}|^2}{8R_{in}} = \frac{|I|^2|Z_{in}|^2}{8R_{in}}, \qquad (39)$$

where P_M is the maximum power available to the load. The magnitudes of Z_{in} and Z_{IC} are the same when they are complex conjugates. Now simply divide the power transferred to the load by the maximum power available to the load to get the power transfer efficiency:

$$\tau = \frac{P_L}{P_M} = \frac{|I|^2|Z_{in}|^2 R_{IC} * 8R_{in}}{2|Z_{in}+Z_{IC}|^2|I|^2|Z_{in}|^2} = \frac{4R_{in}R_{IC}}{|Z_{in}+Z_{IC}|^2}, \qquad (40)$$

where τ is the power transfer efficiency.

The target filter's power transfer efficiency can be calculated for a particular frequency range by using Equation (40) and the element values from Figure 22. The target filter's power transfer efficiency versus frequency is in Figure 24. The target filter's 0.5 dB pass-band appears to range from about 870 MHz to 960 MHz instead of the intended 864 MHz to 954 MHz, but this is close enough for the purpose of showing the concept. This error is likely due to rounding in the filter design calculations.

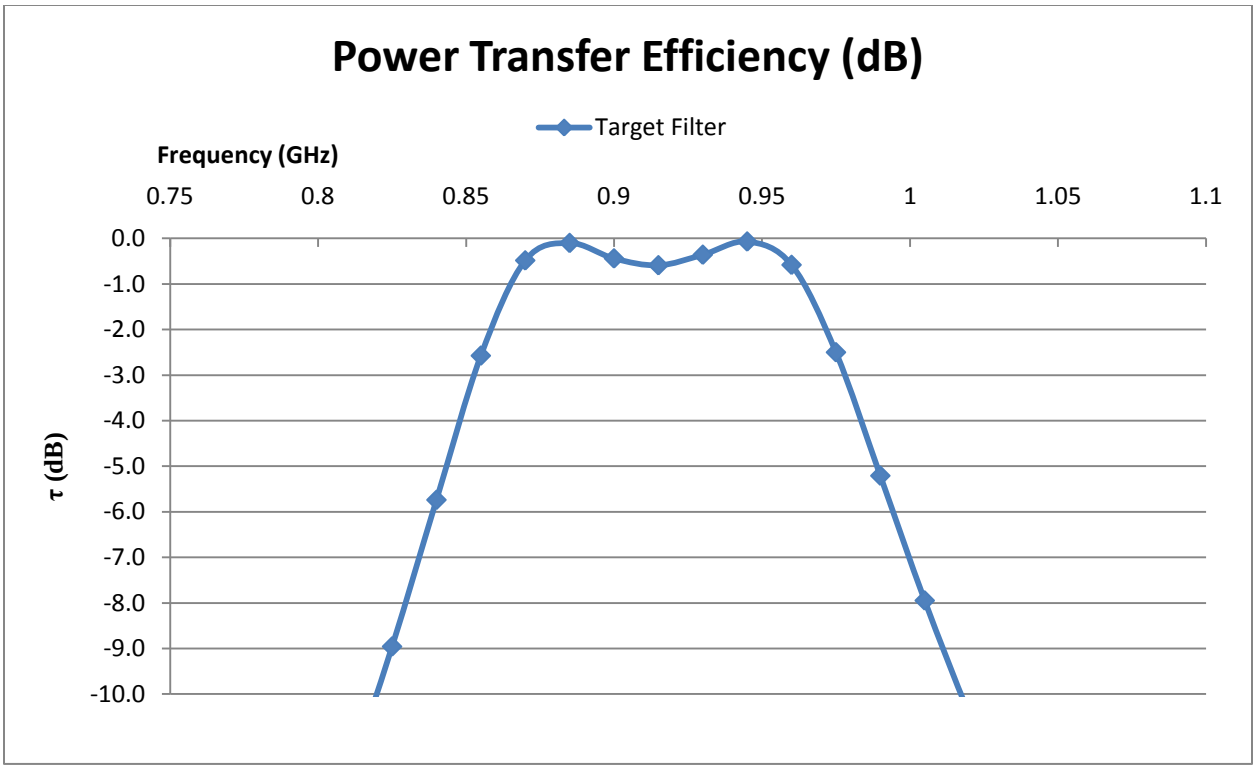

Figure 24: Target Filter Power Transfer Efficiency

4. Commercial Antenna

The second step in designing a T-match antenna that has a band-pass frequency response is designing the antenna itself. A new antenna can be designed or an existing one can be redesigned. For this thesis, on the author chose to redesign an existing antenna. The choice to redesign an existing antenna restricts the design space compared to designing a new antenna. Starting with an existing antenna provides a basic antenna design and features to work with instead of coming up with a completely new design from scratch. Redesigning an existing antenna also allows a comparison to be made between the original commercial antenna and the redesigned antenna to show how much efficiency the redesign adds.

This chapter focuses on a commercial antenna that the author chose for redesign. Section one introduces the commercial antenna that was chosen. The second section shows how to find the antenna's electrical characteristics from Ansoft Designer simulation results. The third section provides the power transfer efficiency measurement for the chosen commercial antenna and compares it with the target filter designed in Chapter 3.

4.1 Commercial Antenna Geometry

The T-match antenna the author chose for re-design is the ALN-9562 Squiggle-SH tag from [19]. The ALN-9562 is a UHF RFID tag antenna that is 19 mm in height and 70 mm long with conductors that are 0.05 mm thick. This antenna was chosen because it has some of the more complex features used in RFID antennas while still being reasonably simple to model in Ansoft Designer. The complexity of the antenna makes the simulation results in this thesis more relatable and useful to other antenna designs.

A 2-port model of this commercial RFID tag antenna was created by the author in Ansoft Designer to simulate its input impedance over the desired frequency range from Chapter 3. The antenna model was changed to attempt to achieve an antenna frequency response identical to the target filter's frequency response in Chapter 3. Figure 25 shows the Ansoft Designer model of the chosen commercial tag next to a picture of the actual tag to show that the model closely matches the original antenna.

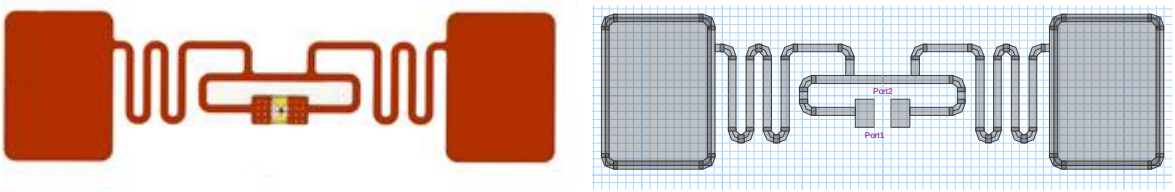

Figure 25: ALN-9562 Squiggle-SH RFID Tag from [19] and its Ansoft Designer Model

4.2 Determining Electrical Characteristics from Simulation Results

In Chapter 3, four electrical characteristics were established that completely characterize the antenna portion of the T-match equivalent circuit: the even-mode resistance R_e, the series resonant frequency ω_0, the series (even-mode) quality factor Q_e, and the odd-mode inductance L_o. Now that an antenna is being simulated, how to determine the values of these four electrical characteristics from simulation results needs to be known.

The even-mode resistance is simply the real part of the even-mode impedance, as stated in Chapter 3. The even-mode impedance can be found from the z-parameters provided by Ansoft Designer using Equations (9) and (12) from Chapter 2. If the even-mode resistance is not constant with frequency, then a good goal during the re-design of the commercial antenna is to

get the resistance near the series resonant frequency equal to R_2 in the target filter circuit in Figure 22.

The series resonant frequency can be found by simply observing the behavior of the even-mode impedance as a function of frequency. The series resonant frequency is the frequency at which the even-mode reactance has a zero-crossing with positive slope.

Equation (37) showed that if the even-mode resistance and the series resonant frequency are known, then only the even-mode inductance is needed to find the series Q. The even-mode inductance can be found from the even-mode impedance by finding the slope of the even-mode reactance at the series resonant frequency. At resonance, a series RLC circuit must have

$$\mathrm{Im}\{Z_e\} = \omega L_e - \frac{1}{\omega C_e} = 0. \qquad (41)$$

Rearranging Equation (41) gives

$$\omega L_e = \frac{1}{\omega C_e}. \qquad (42)$$

Solving for C_e gives

$$\frac{1}{\omega^2 L_e} = C_e. \qquad (43)$$

The result of Equation (43) will be used shortly, but first the derivative of Equation (41) is taken with respect to ω:

$$\frac{d(\mathrm{Im}\{Z_e\})}{d\omega} = \frac{d\left(\omega L_e - \frac{1}{\omega C_e}\right)}{d\omega} = L_e + \frac{C_e}{(\omega C_e)^2} = L_e + \frac{1}{\omega^2 C_e}. \qquad (44)$$

Using Equation (43) to substitute for C_e in Equation (44) results in

$$\frac{d(\mathrm{Im}\{Z_e\})}{d\omega} = L_e + \frac{\omega^2 L_e}{\omega^2} = 2L_e \qquad (45)$$

After using Equation (45) to find L_e, Q_e can be found from Equation (37).

Finally, the odd-mode inductance is simply related to the odd-mode impedance. First, the odd-mode impedance is found from the Ansoft Designer z-parameters using Equation (18) from Chapter 2. Since the odd-mode impedance has practically no real part, the real part can be ignored and the odd-mode inductance is essentially the slope of the odd-mode reactance.

The electrical characteristic values calculated for the original ALN-9562 antenna geometry are in Table 3 beside the target filter electrical characteristic values from Table 2.

Table 3: Original ALN-9562 and Target Filter Electrical Characteristics

Electrical Characteristic	Original ALN-9562	Target Filter
Even-Mode Resistance	194 Ω	504 Ω
Series Resonant Frequency	929 MHz	908 MHz
Series Q	18.2	14.2
Odd-Mode Inductance	23 nH	12.3 nH

Table 3 shows that the commercial antenna characteristics all need to be changed significantly to match the target filter characteristics

A summary of how to calculate the four main electrical characteristics is displayed in Table 4 below. How to change these four characteristics by adjusting T-match antenna geometry features is the focus of the next chapter.

Table 4: Electrical Characteristics Summary

Electrical Characteristic	How to Calculate
Even-Mode Resistance	Real part of even-mode impedance
Series Resonant Frequency	Frequency at which imaginary part of even-mode impedance is 0
Series Q	(Series resonant frequency *even-mode inductance) / even-mode resistance, find even-mode inductance from Equation (45)
Odd-Mode Inductance	Slope of the imaginary part of the odd-mode impedance

4.3 Commercial Antenna Power Transfer Efficiency

Engineers originally designed the ALN-9562 antenna to operate within the desired 864-954 MHz frequency range. The ALN-9562 was designed for use with a specific IC, the Higgs-2, with a resistance of 1500 Ω and a capacitance of 1.2 pF [14]. Figure 26 shows plots of the power transfer efficiencies of the original commercial antenna with its intended IC, the original commercial antenna with the new Monza 4 chip chosen in Chapter 3, and the target band-pass filter. The original antenna does not come close to matching the response of the target filter either with its intended IC or with the new IC. The commercial antenna with the Monza 4 chip has a power transfer efficiency lower than the scale of the graph at most frequencies shown. The graph shows how valuable it will be to design an antenna with the desired frequency response. The bandwidth in which the antenna has low loss will be greatly increased.

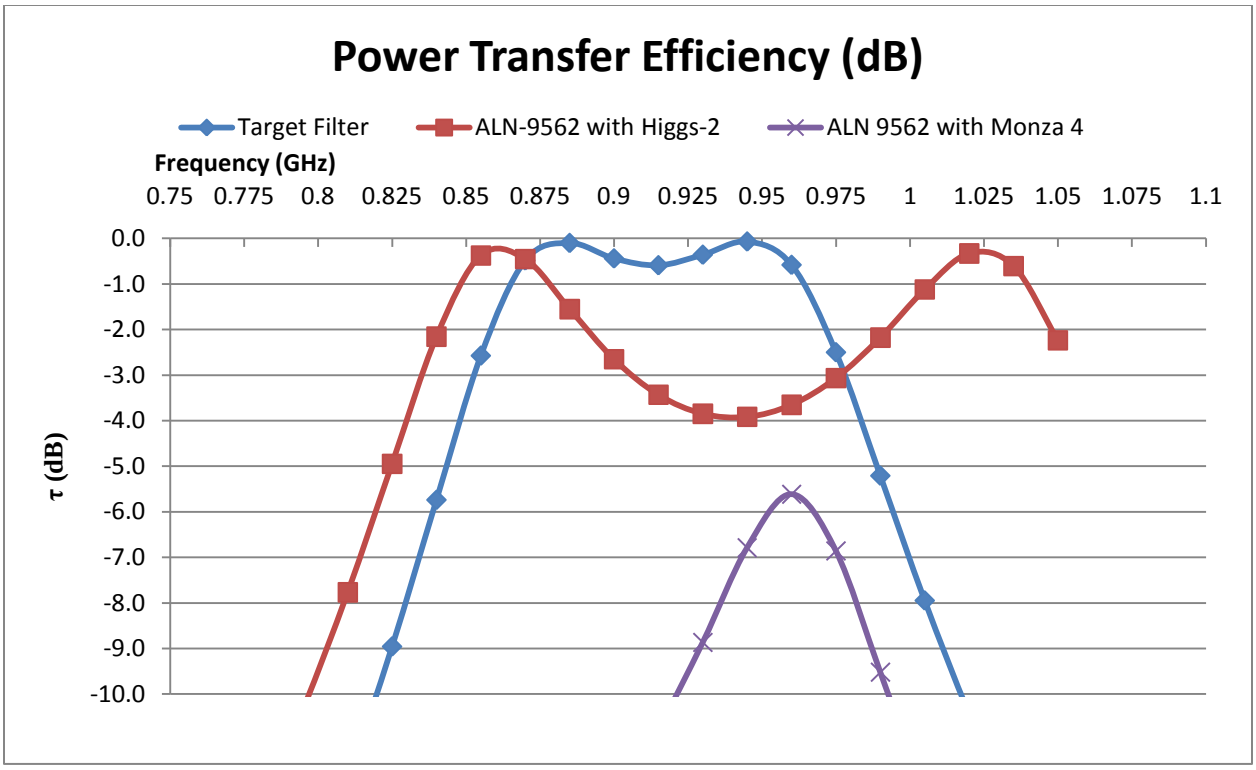

Figure 26: Power Transfer Efficiencies of Original Antenna and Target Band-Pass Filter

Now there is enough information to take the commercial antenna to simulation and redesign it to match the target filter. The next chapter discusses different geometric features that were changed to match the commercial antenna frequency response to that of the target filter. Then, Chapter 6 will show how much more efficient a few antenna redesigns are compared to the original commercial antenna in this chapter.

5. Tuning the Commercial Antenna Geometry

This chapter discusses several T-match antenna geometry features that can be used to tune the T-match antenna's frequency response to be closer to that of a band-pass filter. The author used these features to change the ALN-9562 antenna introduced in Chapter 4 so that its frequency response behaved more like that of the target filter from Chapter 3. All of the data shown in this chapter is from calculations made with data from simulations performed in Ansoft Designer.

The first section of this chapter identifies various tunable feature of the antenna geometry. The next seven sections each focus on a separate tunable feature of the T-match antenna's geometry. These sections start with a reminder of where the feature is located in the antenna geometry along with a figure to illustrate the feature's location. Each section also provides an example tuning of the antenna feature with results calculated from simulation data. Then, more general trends found from the author's simulations are shown for how tuning the antenna feature affects the four main characteristics discussed in section one. The ninth section provides a summary of the tunable antenna geometry features discussed in the other sections. A summary chart is provided with each tunable feature's effects on the antenna's electrical characteristics. The next chapter presents final antenna designs resulting from the tuning of the antenna features discussed in this chapter.

5.1 ALN-9562 Geometric Features

The ALN-9562 antenna geometry has several features that can be varied to change its electrical characteristics. This section identifies many of these tunable features and discusses the antenna geometry in general. The antenna is shown in Figure 27, with all of the tunable features discussed in this chapter identified.

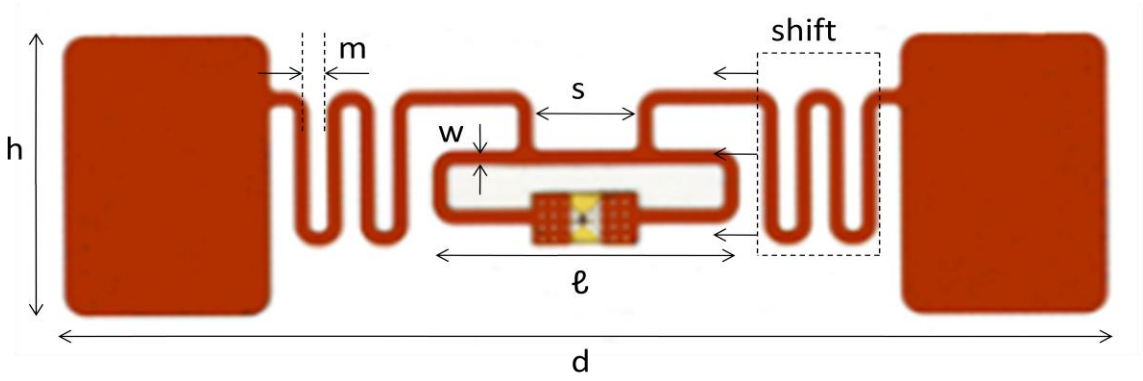

Figure 27: ALN-9562 Squiggle-SH RFID Tag [19] with Tunable Features Identified

The tunable features identified in Figure 27 are listed in Table 5 with a brief description for each feature.

Table 5: Tunable Geometric Features and Brief Descriptions

Tunable Feature	Brief Description	Section
w	Width of the upper conductor of the T-section feed loop	5.2
h	Height of antenna (end-patch and meander heights changed by same amount)	5.3
d	Length of antenna (changed by extending patches on ends outward)	5.4
ℓ	T-section feed loop length	5.5
s	Dipole attachment spacing	5.6
m	Meander spacing	5.7
shift	Horizontal shift of meander positions	5.8

The ALN-9562 antenna is not a simple T-match antenna like that shown in Figure 1. Here, the dipole arms are attached to the T-section feed through vertical traces at the top of the T-section feed loop instead of coming out from the sides of the loop. Instead of having straight dipole arms, the arms meander up and down. The ends of the dipole arms have large conductor squares. These features improve the antenna's performance while keeping it small in size. What exactly each of these features do can be found in RFID texts, such as [1], or in papers that focus on RFID antenna design. The function of some of these features will be identified from their effect on the antenna's electrical characteristics when the geometric features are varied.

The following sections will show how the electrical characteristics in Table 3 change with the geometric features listed in Table 5. The sections also show experimental results and trends for the different geometric features that were varied when re-designing the ALN-9562 antenna.

5.2 T-section Feed Upper Trace Width and R_e

The first useful tunable feature of the T-match antenna geometry found through experimentation was the width *w* of the upper trace of the T-section feed. See Figure 28 for an illustration of where this feature is on the ALN-9562 antenna.

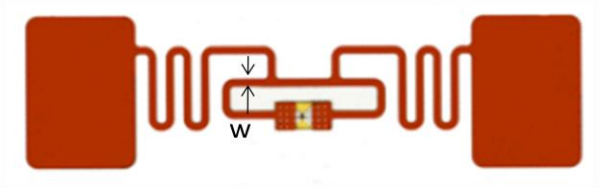

Figure 28: ALN-9562 Antenna with T-section Upper Trace Width w Labeled

The black arrows in Figure 28 mark the width of the upper conductor of the T-section feed and the variable *w* is assigned to this feature. The width *w* was 1 mm for the original, unaltered ALN-9562 antenna, the same width as the rest of the T-section feed loop traces. When changing the width *w*, the width of the traces on the sides and bottom of the T-section feed were not changed. Also, the spacing between the upper and lower conductors of the T-section feed was kept constant.

The geometrical changes for an example case when *w* was changed from 3mm to 5mm are shown in Figure 29.

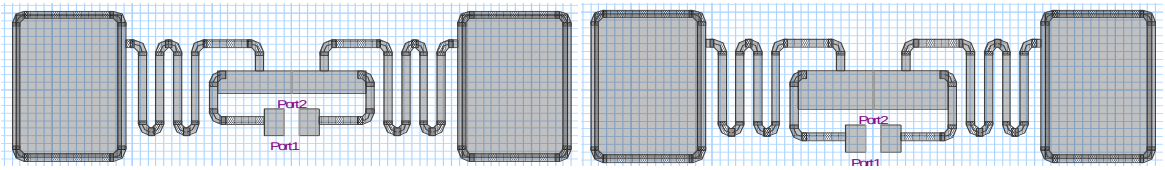

Figure 29: Ansoft Designer Models for the ALN-9562 Antenna for the Cases *w* = 3 mm (left) and *w* = 5 mm (right)

In Figure 29, on the left is a model of the ALN-9562 antenna when *w* = 3 mm and on the right is a model of the ALN-9562 antenna when *w* = 5 mm. As seen in the figure, only the upper trace of the T-section feed was changed. The side and lower traces were left with their original width of 1 mm. In this example, none of the other tunable antenna features had been changed yet.

The effect this change in *w* had on the electrical characteristics is shown in Table 6.

Table 6: Effect of *w* on ALN-9562 Electrical Characteristics from *w* = 3mm to *w* = 5mm

Electrical Characteristic	***w* = 3mm**	***w* = 5mm (+67%)**	**% Change**	**% Change EC / % Increase *w***
Even-Mode Resistance	280 Ω	380 Ω	+35.7	+0.54
Series Resonant Frequency	933 MHz	934 MHz	+0.11	+0.002
Series Q	17.6	17.3	-1.70	-0.03
Odd-Mode Inductance	22.5 nH	24.2 nH	+7.56	+0.11

The first column on the left in Table 6 lists the four main electrical characteristics for the antenna that were being matched to the filter characteristics. The second column from the left shows the electrical characteristic values when *w* = 3 mm. The third column from the left shows the electrical characteristic values when *w* = 5 mm. The fourth column in Table 6 shows the percentage change of each of the four electrical characteristics due to the 2 mm (67%) increase in *w*. The far right column shows the ratios between the percent changes in the electrical characteristics and the percent change in *w*.

Widening the width of the upper trace of the T-section feed primarily increased the even-mode resistance. Table 7 shows this width's average approximate effect on each of the four main electrical characteristics.

Table 7: Average Effect of *w* on ALN-9562 Electrical Characteristics

Electrical Characteristic	**% Change in Characteristic / 1% Increase in *w***
Even-Mode Resistance	+ 0.62
Series Resonant Frequency	+0.001
Series Q	-0.020
Odd-Mode Inductance	+0.07

Table 7 shows that for a 1% increase in *w*, the even-mode resistance increased by approximately 0.62%, the series resonant frequency increased by approximately 0.001%, the series Q decreased by approximately 0.02%, and the odd-mode inductance increased by approximately 0.07%.

Another trend for the change in even-mode resistance that showed less variation was that for every 1mm added to *w*, approximately 50 Ω was added to the even-mode resistance.

The effect that changing *w* had on the antenna's electrical characteristics is reasonable. The reason why can be seen by revisiting Uda's T-match analysis that was shown in Chapter 2. Increasing *w* will increase the magnitude of the splitting factor α that is present in the final form of the T-match equivalent circuit in Figure 18. This was expected, because Uda's original formula for α, while applicable to round wire conductors instead of the planar ones here, showed that α would increase if the ratio between the widths of the upper and lower conductors of the T-section feed increased [3]. The splitting factor has been studied in simulations for the case of planar conductors in [6], where the magnitude of α for planar conductors was found to follow the same general trends as Uda's formula for α with round conductors.

In the T-match equivalent circuit in Figure 18, all of the even-mode impedance components have a factor of $(1 + \alpha)^2$ in them. So if α increases, the resistance and inductance of the RLC model used for the even-mode impedance increase and the capacitance decreases. The fact that this increase in the magnitude of α increases even-mode resistance significantly and does not change the other three electrical characteristics very much makes sense if the rest of the T-match circuit components are considered. The series resonant frequency is inversely proportional to the square root of the product of the even-mode inductance and capacitance, as was shown in Equation (36). If the inductance increases by the same factor that the capacitance decreases, than their product does not change and the series resonant frequency does not change. The series Q from Equation (37) is the series resonant frequency multiplied by the ratio between the series inductance and the series resistance. So, if the series resonant frequency does not change, and the even-mode inductance and resistance change by the same factor, then these

factors cancel in the ratio and the series Q does not change. The odd-mode inductance has nothing to do with α, so it is not affected if α changes.

Table 7 shows that the three characteristics besides the even-mode resistance did change though, even though it was a small change when compared to the even-mode resistance's change. While the change in α theoretically does not alter these characteristics, the change in the antenna dimension *w* has more effect than simply changing α. With the complexities of the antenna geometry, any change in any part of the geometry inevitably affects coupling and current flow in different parts of the antenna, so a small change in the three electrical characteristics besides the even-mode resistance is reasonable.

5.3 Antenna Height and Series Q

The next useful tunable feature of the T-match antenna geometry found through experimentation is the height *h* of the entire antenna, as shown in Figure 30.

Figure 30: ALN-9562 Antenna with Height *h*

The left pair of black arrows in Figure 30 marks the height *h* of the antenna. The right pair of arrows and accompanying dotted lines are illustrating that when the height of the antenna was changed, the heights of the meanders and the end patches were both changed by the same amount. The ends of the T-section feed are not included in this height change, but the dipole

attachments above the T-section feed were changed with the meanders and end patches. The antenna height change was limited by the length of the dipole attachments because they could only get so small before the horizontal dipole conductors touched the T-section feed loop, which would significantly change the antenna behavior.

An example case where the antenna height was changed from 18.5 mm to 18 mm is illustrated in Figure 31.

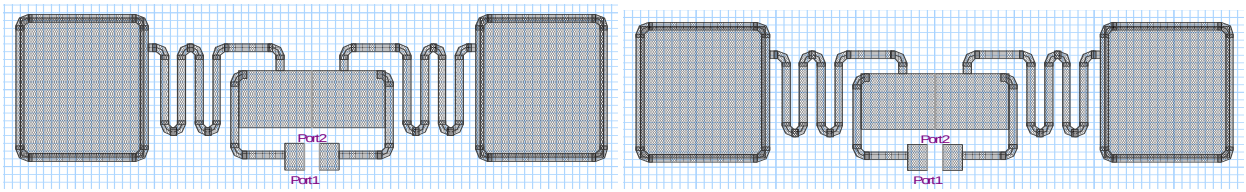

Figure 31: Ansoft Designer Models for the ALN-9562 Antenna for the Cases h = 18.5 mm (left) and h = 18 mm (right)

In Figure 31, the model on the left shows the antenna with a height of 18.5 mm while the model on the right shows the antenna after its height was changed to 18 mm. Prior to this height change, the upper T-section trace width w had been changed to 7.5 mm from 1 mm, the length of the antenna had been changed to 75 mm from 70 mm, and the height had already been decreased to 18.5 mm from 19 mm. As can be seen in the figure, the meander heights and the dipole attachment heights were reduced by the same 0.5 mm by which the end patches were reduced.

The effect that this height change had on the electrical characteristics of the antenna is shown in Table 8.

Table 8: Effect of *h* on ALN-9562 Electrical Characteristics from *h* = 18.5 mm to *h* = 18 mm

Electrical Characteristic	***h* = 18.5 mm**	***h* = 18 mm (-2.7%)**	**% Change**	**% Change EC / % Decrease *h***
Even-Mode Resistance	480 Ω	478 Ω	-0.42	-0.15
Series Resonant Frequency	918 MHz	944 MHz	+2.83	+1.05
Series Q	15.5	13.7	-11.6	-4.30
Odd-Mode Inductance	20 nH	20 nH	+0.00	+0.00

Table 8 is formatted similarly to Table 6 in the previous section. The change in value for each electrical characteristic is shown along with percent changes. The far right column shows the ratio between the percent change in each characteristic and the percent decrease in the height of the antenna.

Changing the height of the antenna significantly affected both the series Q and the series resonant frequency. Table 9 shows the height's average approximate effect on each of the four main electrical characteristics.

Table 9: Average Effect of *h* on ALN-9562 Electrical Characteristics

Electrical Characteristic	**% Change in Characteristic / 1% Decrease in *h***
Even-Mode Resistance	- 0.44
Series Resonant Frequency	+1.14
Series Q	-4.52
Odd-Mode Inductance	+0.10

Table 9 shows that for a 1% decrease in the height of the antenna, its series Q changed the most with a 4.52% decrease on average. The series resonant frequency was also significantly affected with a 1.14% increase on average for every 1% decrease in *h*. The even-mode resistance and odd-mode inductance were not affected as much.

At first glance, it does not seem to make sense that the Q would decrease while at the same time the resonant frequency would increase since the series Q is proportional to the series resonant frequency according to Equation (37) in Chapter 3. A likely explanation for this effect on Q and resonant frequency comes from considering the reduction in overall antenna conductor length that comes from reducing the meander heights.

Reducing a dipole's effective length increases its resonant frequency. This can be found in an antenna text such as [7]. Reducing the height of all the meanders in the antenna reduces the overall conductor length, which reduces the effective length of the antenna. So, it makes sense that the resonant frequency is increasing. Remember from Equation (36) that the series resonant frequency is inversely proportional to the square root of both the even-mode inductance and the even-mode capacitance. Also, in Equation (37), it was shown that the series Q was the series resonant frequency multiplied by the ratio between the even-mode inductance and the even-mode resistance. Taking both equations into consideration, the series Q is essentially proportional to the square root of L_e. Some in the RFID field like to think of any length of conductor as primarily an inductance when dealing with antennas as small as this antenna. This view can be seen in [1] for example. Using this viewpoint, reducing the overall conductor length of the antenna reduces its inductance. If the change in inductance is the most significant change occurring due to the reduction in the antenna height, then the series Q will decrease proportionally to the square root of L_e and the resonant frequency will increase by a similar factor. This explanation does not account for a larger percent decrease in Q than the percent increase in resonant frequency, but it at least makes both occurring at once seem more plausible. The effects caused by the decrease in the antenna's height need to be researched further before it could be said for certain why they are occurring.

5.4 Antenna Length and Series ω_0

Another useful tunable feature that was found for the ALN-9562 antenna is the antenna's length. See Figure 32 for an illustration of where this feature is on the ALN-9562 antenna.

Figure 32: ALN-9562 Antenna with Length *d* Labeled

The length of the antenna was changed by only changing the widths of the two end patches. Each end patch was widened by the same amount outwardly. The length was changed in this way to try and minimize the change in all of the electrical characteristics besides the series resonant frequency.

An example length change is illustrated in Figure 33. This length change was from 70 mm to 75 mm.

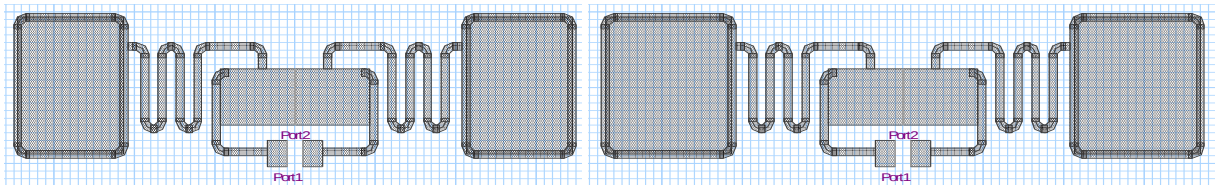

Figure 33: Ansoft Designer Models for the ALN-9562 Antenna for the Cases *d* = 70 mm (left) and *d* = 75 mm (right)

In Figure 33, the model on the left shows the antenna with a length of 70 mm and the model on the right shows the antenna after its length was changed to 75 mm. Prior to this length change,

the upper T-section trace width *w* had been changed to 7.5 mm from 1 mm and the height of the antenna had been changed to 18.5 mm from 19 mm. Figure 33 shows that both end patches were widened by the same amount, which was half of the total length increase.

The effect that this length change had on the electrical characteristics of the antenna is shown in Table 10.

Table 10: Effect of *d* on ALN-9562 Electrical Characteristics from *d* = 70 mm to *d* = 75 mm

Electrical Characteristic	***d* = 70 mm**	***d* = 75 mm (+7.1%)**	**% Change**	**% Change EC / % Increase *d***
Even-Mode Resistance	485 Ω	480 Ω	-1.03	-0.14
Series Resonant Frequency	972 MHz	918 MHz	-5.56	-0.78
Series Q	13.6	15.5	+14.0	+1.96
Odd-Mode Inductance	20.1 nH	20 nH	-0.50	-0.07

Table 10 shows the electrical characteristics for the two different antenna lengths and the percentage of change for each characteristic. The ratios between the percent change for each electrical characteristic and the percent change in length are in the far right column.

Changing the length of the antenna significantly affected both the series Q and the series resonant frequency. Table 11 shows the height's average approximate effect on each of the four main electrical characteristics.

Table 11: Average Effect of *d* on ALN-9562 Electrical Characteristics

Electrical Characteristic	**% Change in Characteristic / 1% Increase in *d***
Even-Mode Resistance	- 0.22
Series Resonant Frequency	-0.79
Series Q	+2.01
Odd-Mode Inductance	-0.07

Table 11 shows that for a 1% increase in the length of the antenna, its series Q changed the most with a 2.01% increase on average. The series resonant frequency was also significantly affected with a 0.79% decrease on average for every 1% decrease in *d*. The even-mode resistance and odd-mode inductance were not affected as much.

An increase in the antenna length would seem to be just a reverse of the decrease in antenna height from the previous section. However, there is one important distinction to be made. An increase in antenna length has a larger ratio between the percent changes in series resonant frequency and series Q than the decrease in antenna height did. An increase in antenna length by 1% produced a percent change ratio of about 0.4 between the series resonant frequency and the series Q while a decrease in antenna height produced a percent change ratio of about 0.24 between the two characteristics. This difference in percent change ratios is important because it means that this length change can be used in conjunction with the height change in the previous section to result in the desired change in both the series resonant frequency and the series Q. For example, the height decrease could be used to get a Q lower than the desired Q first. Then, the length change could be used to get the desired resonant frequency and even though the Q would increase, it would not increase as much as the height change decreased it to begin with in order to get the resonant frequency back where it started. These two features can be changed iteratively until the desired series resonant frequency and Q are both acquired.

Changing the length of the antenna had a similar effect to changing the height of the antenna. Increasing the antenna's length increases its electrical length, and increasing the electrical length lowers the resonant frequency. It can be argued that adding length to the antenna increases the inductance, which in turn would decrease the resonant frequency and increase the Q. See the discussion in the previous section for more details on the relationship

between the inductance, the resonant frequency, and Q. The reasons for the effects from changing the antenna length by widening the end patches would be understood better with more research.

5.5 Length of T-section Feed and L_o

The next useful tunable feature that was found for the ALN-9562 antenna is the length of the T-section feed. See Figure 34 for an illustration of where this feature is on the ALN-9562 antenna.

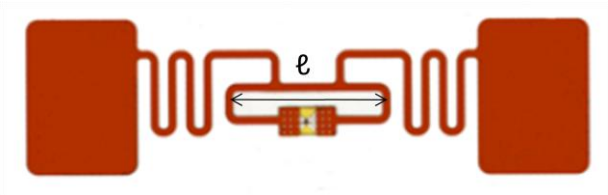

Figure 34: ALN-9562 Antenna with T-section Feed Length ℓ Labeled

The T-section feed length was reduced to reduce the odd-mode inductance. The possible length reduction was limited because the T-section feed has to be long enough for the dipole attachments to stay connected to the top of it.

An example change in ℓ is illustrated in Figure 35. This change in ℓ was from 18.6 mm to 10.6 mm.

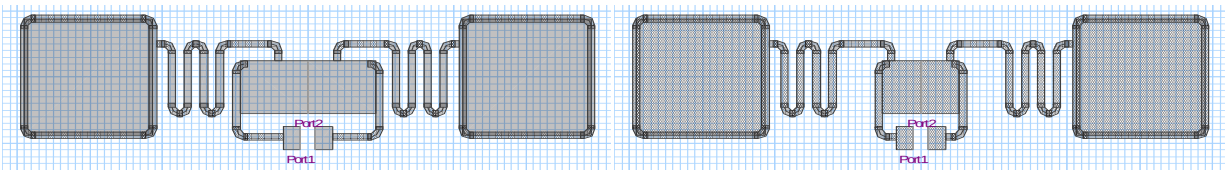

Figure 35: Ansoft Designer Models for the ALN-9562 Antenna for the Cases ℓ = 18.6 mm (left) and ℓ = 10.6 mm (right)

In Figure 35, the model on the left shows the antenna with a T-section feed length of 18.6 mm and the model on the right shows the antenna after its T-section feed length was changed to 10.6 mm. Prior to this T-section feed length change, the upper T-section trace width *w* had been changed to 8 mm from 1 mm, the height of the antenna had been changed to 18 mm from 19 mm, and the antenna length had been changed to 79 mm from 70 mm.

The effect that this T-section feed length change had on the electrical characteristics of the antenna is shown in Table 12.

Table 12: Effect of ℓ on ALN-9562 Electrical Characteristics
from ℓ = 18.6 mm to ℓ = 10.6 mm

Electrical Characteristic	**ℓ = 18.6 mm**	**ℓ = 10.6 mm (-43%)**	**% Change**	**% Change EC / % Decrease ℓ**
Even-Mode Resistance	514 Ω	522 Ω	+1.56	+0.04
Series Resonant Frequency	906 MHz	896 MHz	-1.10	-0.03
Series Q	15	16.1	+7.33	+0.17
Odd-Mode Inductance	19.9 nH	12 nH	-39.7	-0.92

Table 12 shows the electrical characteristics for the two different T-section feed lengths and the percentage of change for each characteristic. The ratios between the percent change for each electrical characteristic and the percent change in T-section feed length are in the far right column.

Changing the T-section feed length of the antenna significantly affected the odd-mode inductance and also affected the even-mode resistance. Table 13 shows the T-section feed length's average approximate effect on each of the four main electrical characteristics.

Table 13: Average Effect of ℓ on ALN-9562 Electrical Characteristics

Electrical Characteristic	% Change in Characteristic / 1% Decrease in ℓ
Even-Mode Resistance	+- 0.42
Series Resonant Frequency	-0.02
Series Q	+0.14
Odd-Mode Inductance	-0.85

Table 13 shows that for a 1% increase in the length of the T-section feed, the odd-mode inductance changed the most with a 0.85% decrease on average. The even-mode resistance was also affected, but sometimes it increased and sometimes it decreased (the +- in Table 13 is not an error). The series resonant frequency and series Q did not change very much.

The reduction in odd-mode inductance due to the reduction in T-section feed length can be explained from the equation for the odd-mode inductance that came from Uda's transmission line assumption discussed in Chapter 2. Equation (22) showed that the odd-mode inductance was approximately proportional to the tangent of half the T-section feed length multiplied by the phase-constant of the transmission lines. As long as the argument of a tangent function is small, the tangent function increases almost linearly as its argument increases. Since ℓ is a factor of the tangent function's argument in Equation (22), it makes sense that the inductance decreases for decreasing ℓ.

5.6 Dipole Attachment Spacing and R_e

Another tunable antenna feature that was useful for changing the even-mode resistance is the spacing between the conductors attaching the dipole arms to the T-section feed loop. An illustration of where this feature is located in the ALN-9562 geometry is shown in Figure 36.

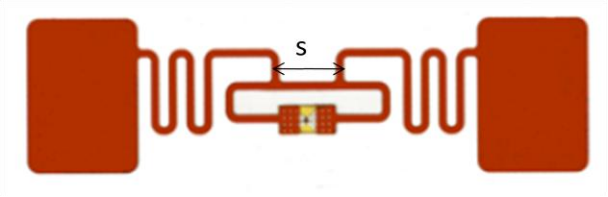

Figure 36: ALN-9562 Antenna with Dipole Attachment Spacing *s* Labeled

The spacing *s* labeled in Figure 36 is reduced by moving the dipole attachments inwards symmetrically. When the spacing *s* is changed, the horizontal conductors above the T-section feed loop are extended inward (if *s* is decreased) or reduced in length (if *s* is increased) by the same amount that the spacing s is changed. The reduction in *s* that is possible is limited because the dipole attachments cannot touch each other.

An example case where *s* was changed is illustrated in Figure 37. In the example, *s* was reduced from its original value of 7.1 mm to 5.1 mm.

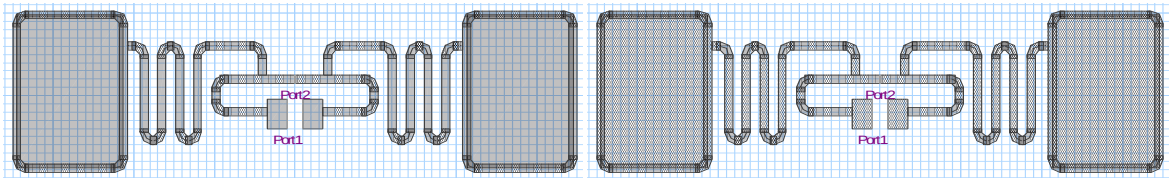

Figure 37: Ansoft Designer Models for the ALN-9562 Antenna for the Cases *s* = 7.1 mm (left) and *s* = 5.1 mm (right)

In Figure 37, the left model is for the case of *s* = 7.1 mm and the right model is for the case of *s* = 5.1 mm. No other changes had been made to the original ALN-9562 geometry before this change in *s* was simulated.

The effect that this change in *s* had on the antenna's electrical characteristics is shown in Table 14.

Table 14: Effect of *s* on ALN-9562 Electrical Characteristics from *s* = 7.1 mm to *s* = 5.1 mm

Electrical Characteristic	***s* = 7.1 mm**	***s* = 5.1 mm (-28%)**	**% Change**	**% Change EC / % Decrease *s***
Even-Mode Resistance	194 Ω	251 Ω	+29.4	+1.04
Series Resonant Frequency	944 MHz	937 MHz	-0.74	-0.03
Series Q	16.3	16.2	-0.61	-0.02
Odd-Mode Inductance	22.7 nH	22.8 nH	+0.44	+0.02

Table 14 shows that the electrical characteristic changes for the example change in *s* were not very significant except for the even-mode resistance. The starting values for the electrical characteristics in Table 14 are slightly different from those listed in Table 5.2.2 for the original ALN-9562 antenna. This is because slightly different settings in Ansoft Designer were being used at this time compared to those being used when the values in Table 5.2.2 were found. These slight settings changes caused more difference in the antenna's starting electrical characteristic values than they did in the values for the final antenna designs in the next chapter.

Changing the spacing between the dipole attachments primarily affected the even-mode resistance. This spacing's approximate effect on the antenna's electrical characteristics is shown in Table 15.

Table 15: Average Effect of *s* on ALN-9562 Electrical Characteristics

Electrical Characteristic	**% Change in Characteristic / 1% Decrease in *s***
Even-Mode Resistance	+1.11
Series Resonant Frequency	-0.02
Series Q	-0.03
Odd-Mode Inductance	+0.01

Table 15 shows that the even-mode resistance was the only electrical characteristic that was significantly affected by a change in the spacing *s*.

The effects from changing the dipole attachment spacing are reasonable if the T-match equivalent circuit resulting from the lumped circuit analysis in Chapter 2 is considered. The scaling factor β is proportional to the ratio between the total inductance of the T-section feed loop and the inductance due to the portion of the T-section feed loop inside the dipole attachments. Decreasing *s* decreases the inductance between the dipole attachments and thus increases the scaling factor β. β is multiplied by all of the elements of the T-match equivalent circuit in Figure 15, and its square is multiplied by some of the elements. This means that an increase in β should increase the even-mode resistance and the odd-mode inductance. Simulations showed a negligible increase in odd-mode inductance though, which means there is likely more happening than just the increase in β due to the change in dipole attachment spacing.

5.7 Meander Spacing

The last two tunable features discussed in this chapter were chosen more for aesthetics than for their usefulness in changing the antenna's electrical characteristics. For these two features, more research is needed to understand why their changes had the effects that they did. The first of these features is the spacing between the meanders. An illustration of the location of this feature is shown in Figure 38.

Figure 38: ALN-9562 Antenna with Meander Spacing *m* Labeled

The spacings between all the meanders were changed at the same time. The overall length of the antenna was not changed. The spacings between the end patches and the first meanders on each end were not changed either. The meanders were spread out evenly towards the center of the antenna as will be seen in the example shown shortly. The meander spacing was chosen for study because when the T-section feed length is decreased to get the desired odd-mode inductance like in Section 5.6, it leaves a large open space between the ends of the T-section feed loop and the first meander. Spreading out the meanders was an attempt to get rid of the huge gaps between the meanders and the T-section feed.

Only a couple of simulations were done for this feature because its purpose was primarily for aesthetics and not for getting the antenna to behave more like a band-pass filter. Not enough simulations were done to provide good approximate averages, so only an example is shown. Figure 39 shows an illustration of the example case where the meander spacing was increased from its original distance of 1.2 mm to 2.2 mm.

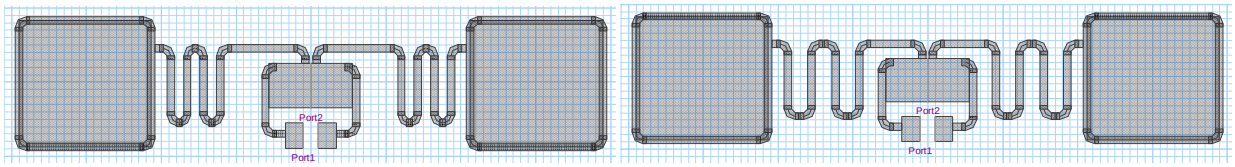

Figure 39: Ansoft Designer Models for the ALN-9562 Antenna for the Cases m = 1.2 mm (left) and m = 2.2 mm (right)

In Figure 39, the model on the left shows the case where m = 1.2 mm and the model on the right shows the case where m = 2.2 mm. Before this change was made, a number of other changes had already been made to the original antenna. The dipole attachment spacing s was reduced to 0.5 mm from 7.1 mm, the T-section feed length ℓ was reduced to 11.1 mm from 18.6 mm, the height

h of the antenna was reduced to 17.5 mm from 19 mm, the T-section feed upper conductor width *w* was increased to 6 mm from 1 mm, and the antenna length *d* was increased to 79 mm from 70 mm.

The effect that this change in *m* had on the antenna's electrical characteristics is shown in Table 16.

Table 16: Effect of *m* on ALN-9562 Electrical Characteristics from *m* = 1.2 mm to *m* = 2.2 mm

Electrical Characteristic	***m* = 1.2 mm**	***m* = 2.2 mm (+83%)**	**% Change**	**% Change EC / % Increase *m***
Even-Mode Resistance	530 Ω	370 Ω	-30.2	-0.36
Series Resonant Frequency	909 MHz	895 MHz	-1.54	-0.02
Series Q	15	17	+13.3	+0.16
Odd-Mode Inductance	12 nH	11.9 nH	-0.83	-0.01

Table 16 shows that the most significant change due to the increase in *m* was a decrease in the even-mode impedance. The series Q also had a somewhat significant change, but the remaining two electrical characteristics did not change much. If the meander spacing were to be changed in order to fill gaps in the antenna geometry, then obviously the adverse effects that it causes to the antenna's electrical characteristics would have to be corrected. Because of this, changing the meander spacing may not be worth the extra work required afterwards.

5.8 Meander Shift

The second tunable feature that was more for aesthetic purposes than anything else is a shift in the meander position in relation to the rest of the antenna. An illustration of this feature's location is shown in Figure 40.

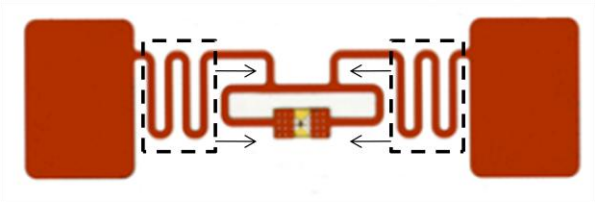

Figure 40: ALN-9562 Antenna with Meander Shift Shown

The idea illustrated in Figure 40 is that the meanders (in the dashed boxes) are shifted inwards towards the T-section feed and away from the end patches. In the figure, there does not appear to be enough room for much of a shift, but this shift was meant more for cases where the T-section feed length has already been reduced significantly.

Only a couple of simulations were done for this feature because, similar to the feature in the previous section, its purpose was primarily for aesthetics and not for getting the antenna to behave more like a band-pass filter. Not enough simulations were done to provide good approximate averages, so only an example is shown. Figure 41 illustrates an example case where the meanders were shifted 2 mm inwards towards the T-section feed.

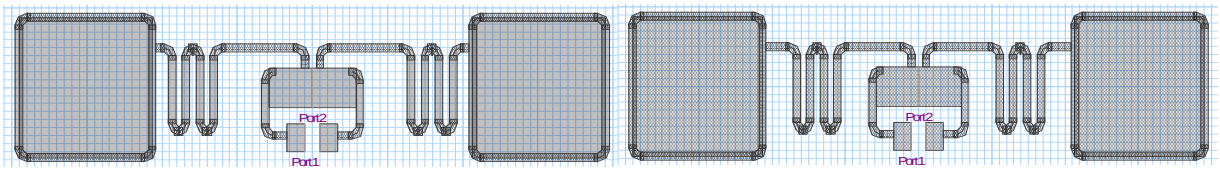

Figure 41: Ansoft Designer Models for the ALN-9562 Antenna for the Cases with no meander shift (left) and with a 2 mm meander shift (right)

In Figure 41, the model on the left has the meanders in their original location and the model on the right has the meanders shifted 2 mm inwards towards the T-section feed. Prior to this meander shift, the attachment spacing *s* was decreased to 1 mm from 7.1 mm, the T-section feed

length ℓ was decreased to 11.6 mm from 18.6 mm, the height of the antenna was decreased to 18 mm from 19 mm, the antenna length *d* was increased to 79 mm from 70 mm, the T-section feed upper conductor width *w* was increased to 5 mm from 1 mm, and the meander spacing *m* was reduced by 1 mm from 1.2 mm.

The effect that this meander shift had on the antenna's electrical characteristics is shown in Table 17.

Table 17: Effect of a 2mm meander shift on ALN-9562 Electrical Characteristics

Electrical Characteristic	No shift	2mm shift	% Change
Even-Mode Resistance	514 Ω	462 Ω	-10.1
Series Resonant Frequency	909 MHz	903 MHz	-0.66
Series Q	14.6	15.4	+5.48
Odd-Mode Inductance	12.4 nH	12.4 nH	+0.00

Table 17 does not include a column for the ratio between the percent change in electrical characteristic and the percent change in shift because there is not really a way to have a percent change in shift. The most significant change in the electrical characteristics was the decrease in even-mode resistance. There was also a somewhat significant increase in the series Q. More research needs to be done before the reasons for these changes can be fully understood.

5.9 Tunable Features Summary

The approximate average effects of each tunable feature on all four main electrical characteristics of the antenna have been compiled into Table 18.

Table 18: Tunable Features' Effects on Antenna Electrical Characteristics in %

Tunable Feature	R_e	Series ω_0	Series Q	L_o
1% increase in *w*	**+ 0.62**	+0.001	-0.020	+0.07
1% decrease in *h*	-0.44	**+1.44**	**-4.52**	+0.10
1% increase in *d*	-0.22	**-0.79**	**+2.01**	-0.07
1% decrease in ℓ	+-0.42	-0.02	+0.14	**-0.85**
1% decrease in *s*	**+1.11**	-0.02	-0.03	+0.01
1% increase in *m*	-0.36	-0.02	+0.16	-0.01

For each antenna electrical characteristic in Table 18, the two tunable features that caused the most percent change are in bold. The meander shift feature is not included in the table because there was no way to calculate a percentage in meander shift. In order to get the antenna to behave like the target filter, just choose the applicable tunable feature for a characteristic that needs changing from Table 18 and change it until the desired characteristic value is reached. Then, choose another characteristic that needs changing and do the same thing. Repeat this process until all of the antenna characteristics are approximately matching the target filter characteristics. The next chapter shows a couple of example designs that started with the commercial antenna discussed in this paper and made use of the tunable features in Table 18. There are sure to be other features on the antenna that can be changed to get desired electrical characteristics other than the ones discussed in this chapter, but the ones in this chapter were the only ones researched in order to show the design concepts in this paper.

6. Efficient Antenna Designs

This chapter presents three antenna designs that were realized using the tunable antenna features in Chapter 5 to redesign the commercial antenna in Chapter 4. The commercial antenna was re-designed so that it would have a frequency response (power transfer efficiency) as close as possible to the target filter designed in Chapter 3. The three antenna designs were simulated in Ansoft Designer to find their frequency responses.

The first three sections each present one of the three antenna designs as well as insights drawn from the antenna design. A summary table in each section lists the changes made to the tunable antenna features from Chapter 5 to get the final antenna design. Each section also compares a power transfer efficiency curve for the antenna design to the target filter's curve. The fourth section compares the power transfer efficiencies of the antenna designs in the first three sections to that of the original ALN-9562 antenna. It also covers some of the good and bad qualities of the antenna designs from the first three sections.

6.1 Antenna Design 1

For the first antenna design, four of the tunable antenna features discussed in the previous chapter were used, one tunable feature for each electrical characteristic. Using a minimum number of tunable features helps keep the design process relatively simple and quick. The four features used are the T-section feed upper trace width w, the antenna height h, the antenna length d, and the T-section feed length ℓ. Figure 42 shows the geometries of the original ALN-9562 antenna and Antenna Design 1 side by side for comparison.

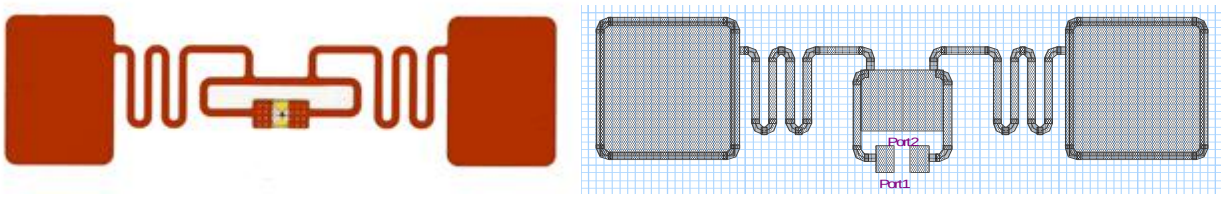

Figure 42: Antenna Geometries for Original ALN-9562 (left) and Antenna Design 1 (right)

Table 19 summarizes the details for the geometry changes made in Antenna Design 1. First, the T-section feed upper trace width *w* was changed to get the even-mode resistance close to its target value of 504 Ω. Next, the antenna height *h* and length *d* were changed, starting with the height *h* being reduced to lower the series Q, and followed by lengthening *d* to reduce the series resonant frequency. *h* and *d* were alternated between since both had significant effects on the series Q and resonant frequency. Then, *w* was increased again to counteract the decrease in even-mode resistance from changing *h* and *d*, followed by a small change in *d* to more finely tune the series resonant frequency. The last of the four tunable features changed was the T-section feed length ℓ, which was decreased in order to reduce the odd-mode inductance. The antenna length *d* was reduced after decreasing ℓ to correct for the series resonant frequency.

In Table 19, the first column at the left lists the tuning step. In the top half of the table, the next four columns have the values for each of the four tunable antenna features used in this design that correspond to the tuning step in the first column. For detailed descriptions of these features see Chapter 5. The values with percentages in parenthesis indicate that the feature was changed by the percentage in parenthesis for the corresponding tuning step. The four rightmost columns in the bottom half of the table list the values for the electrical characteristics for each tuning step with their percent changes in parenthesis if they changed. The step zero row

indicates the original antenna feature and characteristic values. The bottom row shows the target filter values.

Table 19: Tuning Steps Taken for Antenna Design 1

	Tunable Antenna Features			
Step	**w (mm)**	**h (mm)**	**d (mm)**	**ℓ (mm)**
0	1	19	70	18.6
1	7.5 (+650%)	19	70	18.6
2	7.5	18.5 (-2.6%)	70	18.6
3	7.5	18.5	75 (+7.1%)	18.6
4	7.5	18 (-2.7%)	75	18.6
5	7.5	18	78 (+4%)	18.6
6	8 (+6.7%)	18	78	18.6
7	8	18	79 (+1.3%)	18.6
8	8	18	79	10.6 (-43%)
9	8	18	78 (-1.3%)	10.6
	Electrical Characteristics			
Step	**R_e (Ω)**	**ω_0 (MHz)**	**Q**	**L_o (nH)**
0	194	929	18.2	22.9
1	484 (+149.5%)	944 (+1.6%)	15.3 (-15.9%)	20 (-12.7%)
2	485 (+0.2%)	972 (+3%)	13.6 (-11.1%)	20.1 (+0.5%)
3	480 (-1%)	918 (-5.6%)	15.5 (+14%)	20 (-0.5%)
4	478 (-0.4%)	944 (+2.8%)	13.7 (-11.6%)	20
5	475 (-0.6%)	915 (-3%)	14.6 (+6.6%)	19.9 (-0.5%)
6	515 (+8.4%)	915	14.6	19.9
7	514 (-0.2%)	906 (-1%)	15 (+2.7%)	19.9
8	522 (+1.6%)	896 (-1.1%)	16.1 (+7.3%)	12 (-39.7%)
9	524 (+0.4%)	905 (+1%)	15.7 (-2.5%)	12
Target	504	908	14.2	12.3

Figure 42 and Table 19 show that Antenna Design 1 is longer end-to-end and slightly shorter in height compared to the original commercial antenna. Antenna Design 1 also has a much wider T-section feed upper trace width and a much shorter T-section feed length than the original antenna had. These changes created more empty space between the T-section feed and the meanders and also turned the T-section feed upper trace into more of a patch than just a trace. This extra space and small patch give a somewhat undesirable appearance to Antenna Design 1 and do not use space as efficiently as the original commercial antenna did. Also, the driven port

of the antenna sticks out below the rest of the antenna. If efficient use of space is a major concern, then this minimalist approach of only using four tunable features is not the best choice.

The antenna design electrical characteristics do not perfectly match those of the target filter, but they are close. The power transfer efficiencies of both Antenna Design 1 and the target filter are in Figure 43.

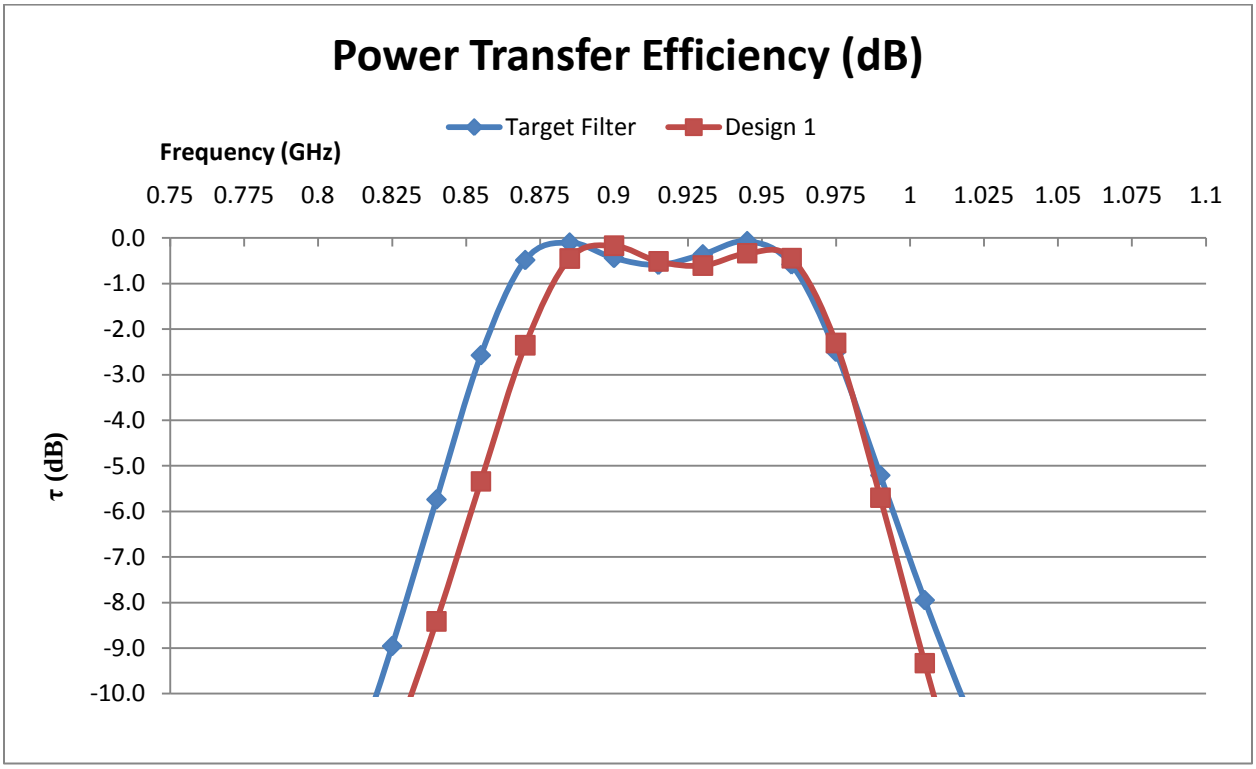

Figure 43: Power Transfer Efficiencies for Antenna Design 1 and the Target Filter

Figure 43 shows that the frequency response of Antenna Design 1 was close to that of the target filter. Antenna Design 1 has a narrower bandwidth than the target filter. Antenna Design 1 has a 0.5 dB pass-band ranging from about 885 MHz to about 960 MHz, while the target filter pass-band ranges from 870 MHz to 960 MHz. This is likely because the series Q in Design 1 is higher than that of the target filter. Section 6.4 will show that while Design 1 does not perfectly

match the target filter's response, it certainly has a much wider bandwidth in which the power transfer efficiency is high compared to the original commercial antenna.

6.2 Antenna Design 2

For Antenna Design 2, the four tunable features used in Design 1 were used, but the dipole attachment spacing s was also changed in order to attempt to address the T-section feed upper trace width issue from Antenna Design 1. The antenna geometry for Antenna Design 2 is shown in Figure 44.

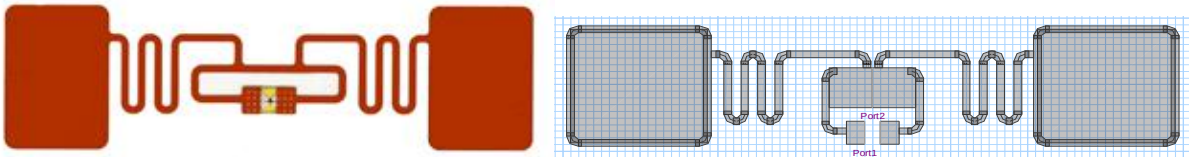

Figure 44: Antenna Geometries for Original ALN-9562 (left) and Antenna Design 2 (right)

Table 20 summarizes the details for the geometry changes made in Antenna Design 2. The even-mode resistance was changed as much as possible by decreasing *s* before turning back to *w* to finish the job. The T-section feed length ℓ was decreased after the initial change in *s* in order to see how much it nullified the effect of decreasing *s*. After as much even-mode resistance increase as possible was squeezed out of the dipole spacing *s*, the T-section feed upper trace width *w* still needed to be increased some to get near 504 Ω. The features *w*, *h*, and *d* were then changed, often two at a time since their effects were understood reasonably well after Antenna Design 1, to get the even-mode resistance, series Q, and resonant frequency close to their target values.

Table 20: Tuning Steps Taken for Antenna Design 2

	Tunable Antenna Features				
Step	**w (mm)**	**h (mm)**	**d (mm)**	**ℓ (mm)**	**s (mm)**
0	1	19	70	18.6	7.1
1	1	19	70	18.6	1.1 (-84.5%)
2	1	19	70	11.6 (-37.6%)	0.8 (-27.3%)
3	1	19	70	10.6 (-8.6%)	0.5 (-37.5%)
4	1	19	70	9.6 (-9.4%)	0.5
5	5 (+400%)	19	70	11.1 (+15.6%)	0.5
6	4.5 (-10%)	19	72 (+2.9%)	11.1	0.5
7	4.5	18 (-5.3%)	72	11.1	0.5
8	4.5	18	77 (+6.9%)	11.1	0.5
9	5 (+11%)	17.5 (-2.8%)	77	11.1	0.5
10	6 (+20%)	17.5	79 (+2.9%)	11.1	0.5

	Electrical Characteristics			
Step	**R_e (Ω)**	**ω_0 (MHz)**	**Q**	**L_o (nH)**
0	194	944	16.3	22.7
1	484 (+149.5%)	926 (-1.9%)	15.8 (-3.1%)	22.9 (+0.9%)
2	401 (-17.1%)	928 (+0.2%)	16.3 (+3.2%)	14.2 (-38%)
3	407 (+1.5%)	928	16.3	13 (-8.5%)
4	375 (-7.9%)	929 (+0.1%)	16.6 (+1.8%)	11.7 (-10%)
5	551 (+46.9%)	927 (-0.2%)	16.6	12 (+2.6%)
6	519 (-5.8%)	908 (-2%)	17.9 (+7.8%)	12.1 (+0.8%)
7	475 (-8.5%)	956 (+5.3%)	14 (-21.8%)	12.1
8	467 (-1.7%)	905 (-5.3%)	16.1 (+15%)	12 (-0.8%)
9	469 (+0.4%)	928 (+2.5%)	14.3 (-11.2%)	12
10	530 (+11.5%)	909 (-2%)	15 (+4.9%)	12
Target	504	908	14.2	12.3

Table 20 has a layout similar to that of Table 19, except that it has an extra tunable feature in the top half of the table. The tunable feature values and electrical characteristic values are shown for each design step, and the values that changed have a percentage change value in parenthesis next to them.

Similar to Antenna Design 1, Antenna Design 2 is longer end-to-end and shorter in height than the original commercial antenna. The T-section feed upper trace width still had to increase some because the decrease in dipole attachment spacing was limited to keep the attachments from touching each other. If the dipole attachments touched, it may not prove to be a large issue,

but then again it may significantly change the operation of the antenna. In order to avoid the latter possibility, the attachments were not allowed touch. While the T-section feed upper trace width was still increased, it no longer causes the driven port of the antenna to stick out below the rest of the antenna like it did in Antenna Design 1.

The power transfer efficiency for Antenna Design 2 is plotted in Figure 45 along with the target filter power transfer efficiency.

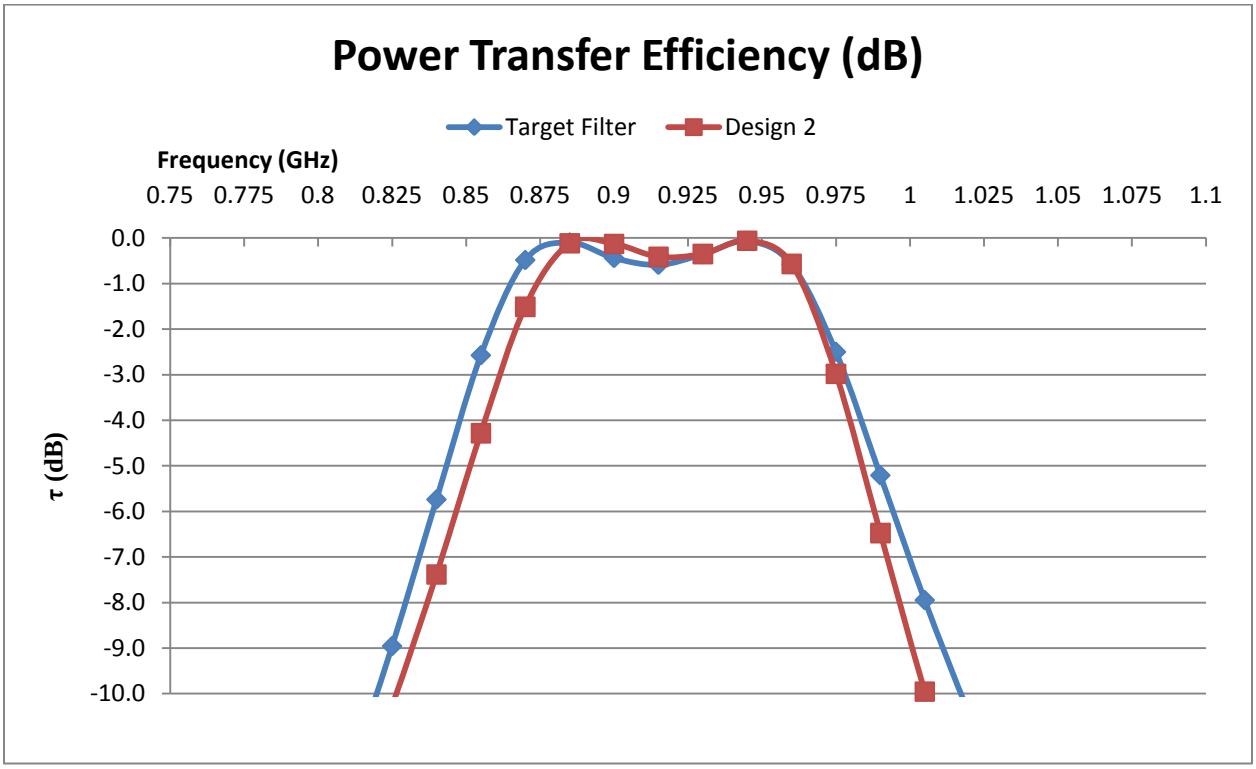

Figure 45: Power Transfer Efficiencies for Antenna Design 2 and the Target Filter

Figure 45 shows that Antenna Design 2's frequency response is close to that of the target filter. Antenna Design 2's response is narrower in bandwidth than the target filter's response, similar to Antenna Design 1. Antenna Design 2's 0.5 dB pass-band ranges from about 878 MHz to about 960 MHz compared to the target filter's pass-band from 870 MHz to 960 MHz. Section 6.4 will

compare Antenna Design 2's power transfer efficiency to the original antenna's and show that Antenna Design 2 has a much wider bandwidth in which there is high power transfer efficiency.

6.3 Antenna Design 3

Antenna Design 3 started from Antenna Design 2, and then the meander spacing m and meander shift tunable features were used to attempt to better distribute the antenna's use of space. The antenna geometry for Antenna Design 3 is shown in Figure 46.

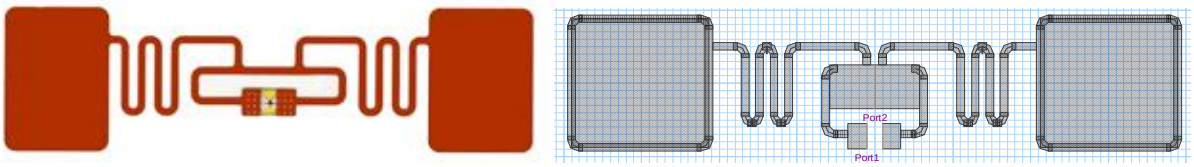

Figure 46: Antenna Geometries for Original ALN-9562 (left) and Antenna Design 3 (right)

Table 21 summarizes the details for the geometry changes made in Antenna Design 3. First, the dipole attachment spacing *s* was increased slightly to have a reasonable gap width between the attachments, and the meander spacing was reduced in order to reduce Q. Then, several of the other tunable features used in the previous designs were changed to try and correct for the unwanted effects of changing the meander spacing. Next, the meanders were shifted so that they were more centered between the end patches of the antenna and the T-section feed loop. This significantly reduced the even-mode resistance, so *w* was increased to compensate. Table 21 starts with tuning step 10 as a continuation from Table 20. The format of Table 21 is similar to that of Tables 19 and 20 with additional tunable features in the top half of the table.

Table 21: Tuning Steps Taken for Antenna Design 3

	Tunable Antenna Features						
Step	**w (mm)**	**h (mm)**	**d (mm)**	**ℓ (mm)**	**s (mm)**	**m (mm)**	**shift (mm)**
10	6	17.5	79	11.1	0.5	1.2	0
11	6	17.5	79	11.1	1 (+100%)	0.87 (-27.5%)	0
12	5(-16.7%)	18 (+2.9%)	79	11.6 (+4.5%)	1	0.87	0
13	5	18	79	11.6	1	0.87	2
14	6 (+20%)	18	79	11.6	1	0.87	2

	Electrical Characteristics			
Step	**R_e (Ω)**	**ω_0 (MHz)**	**Q**	**L_o (nH)**
10	530	909	15	12
11	566 (+6.8%)	932 (+2.5%)	13 (-13.3%)	11.9 (-0.8%)
12	514 (-9.2%)	909 (-2.5%)	14.6 (+12.3%)	12.4 (+4.2%)
13	462 (-10.1%)	903 (-0.7%)	15.4 (+5.5%)	12.4
14	531 (+14.9%)	903	15.5 (+0.6%)	12.6 (+1.6%)
Target	504	908	14.2	12.3

Antenna Design 3 is longer end-to-end and shorter in height than the original commercial antenna, much like the previous two antenna designs. The significant differences from the other previous designs are that the meander spacing has been decreased and the meanders have been shifted inwards towards the T-section feed. The original intent with this antenna design was to increase the meander spacing to make better use of space as opposed to decreasing the meander spacing. The reason the spacing was decreased instead of increased is because decreasing the meander spacing lowered the series Q, which was more desirable from a functional standpoint than increasing the meander spacing. Also, this decrease in Q proved valuable when corrections for other electrical characteristics were made and the meanders were shifted later because these other geometry changes caused the Q to increase somewhat significantly. The antenna's empty space was still able to be re-distributed some due to the meander shift, giving the Antenna Design 3 a better appearance than Antenna Design 2.

The power transfer efficiency of Antenna Design 3 is in Figure 47 along with the target filter power transfer efficiency.

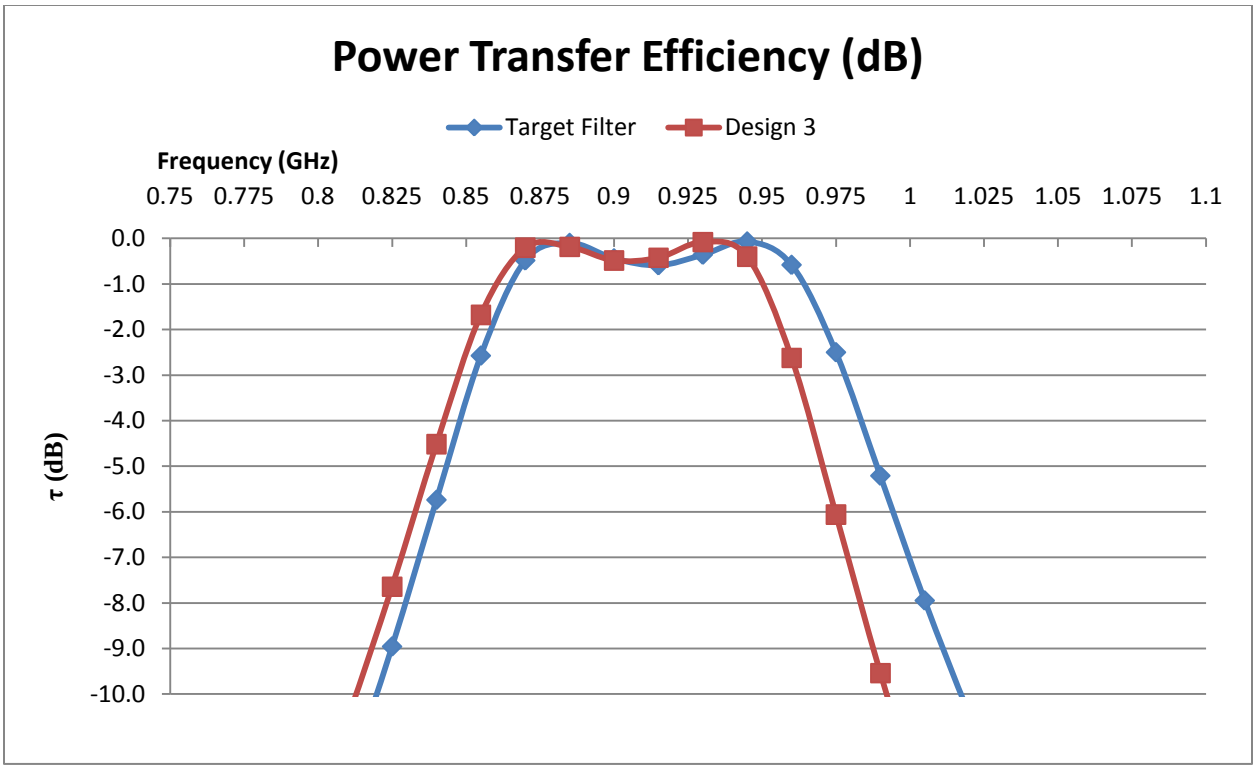

Figure 47: Power Transfer Efficiencies for Antenna Design 3 and the Target Filter

Antenna Design 3's frequency response in Figure 47 is shifted lower in frequency than the target filter's response. Antenna Design 3's pass-band ranges from about 865 MHz to about 948 MHz compared to the target filter's pass-band from 870 MHz to 960 MHz. For this antenna design, the even-mode impedance and series Q are higher than the target filter's and the series resonant frequency is slightly lower than the target filter's. These differences cause the shift in frequency and narrower bandwidth. The next section will compare Antenna Design 3's power transfer efficiency to that of the original commercial antenna and show that the new design's efficient bandwidth has increased compared to the original antenna.

6.4 Antenna Designs vs. Original Antenna

The antenna designs in the previous three sections came close to matching the frequency response of the target filter from Chapter 3. The power transfer efficiencies of these antennas are plotted together in Figure 48 for comparison.

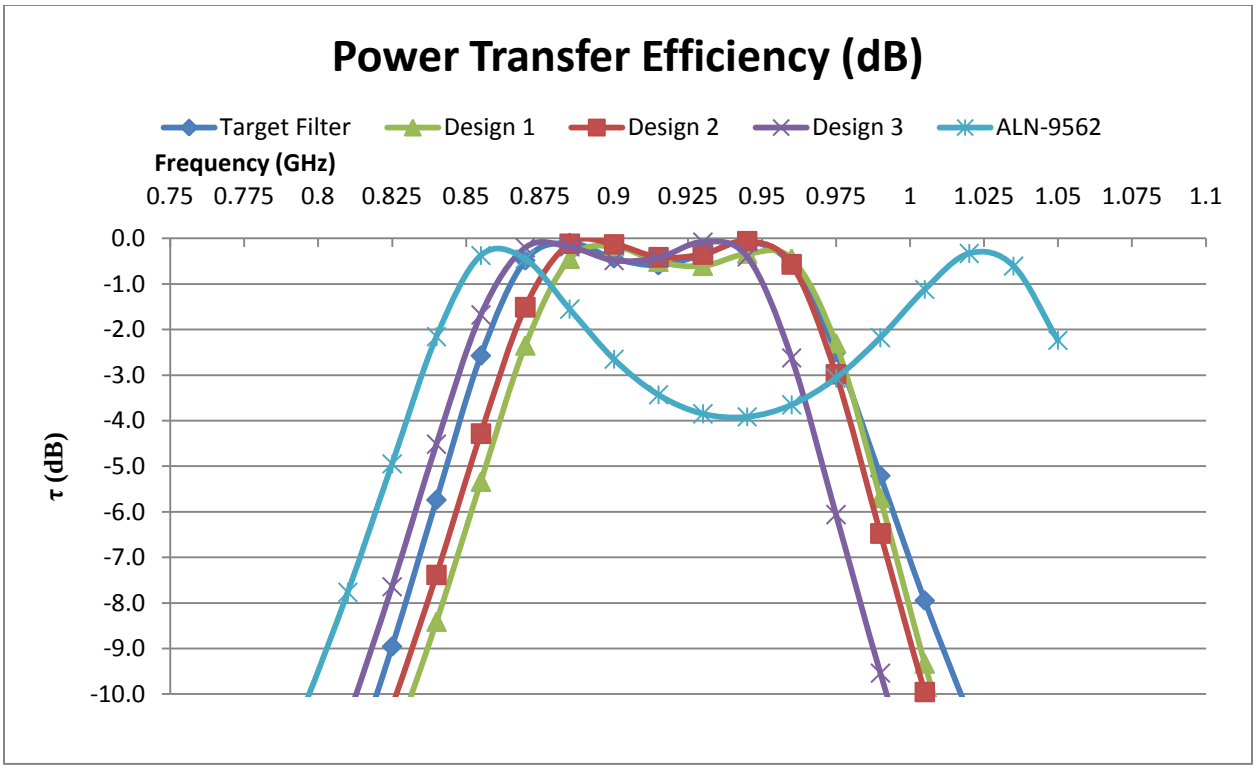

Figure 48: Power Transfer Efficiencies of the Target Filter, Antenna Design 1, Antenna Design 2, Antenna Design 3, and the Original ALN-9562 Antenna

Figure 48 shows that all of the antenna designs from this chapter have frequency responses closer to the target filter than the original ALN-9562 antenna did. The new designs have a much wider 0.5 dB bandwidth than the original antenna. None of the new designs match the target filter perfectly, but if they were tuned more precisely, then they could be made to match better. For the purposes of this thesis, more precise tuning was not needed. The present forms of these

antenna designs show that T-match antennas can be designed to have frequency responses similar to band-pass filters.

The greater efficiency that the three antenna designs in this chapter have compared to the original commercial antenna has benefits for the use of UHF RFID tags. Greater power transfer efficiency means that less power is lost between an RFID tag receiving a signal and sending its response. With more power available for the tag's response, the tag could potentially be used from farther away and still meet the received signal power requirements of the reader. Instead of using the greater efficiency for added read distance, the power transmitted by the reader to read a tag at a particular distance could be decreased. This in turn may help reduce the cost of the RFID reader needed.

An important consideration when it comes to RFID tag antennas is the physical size of the antenna. There is often a specified area that an RFID tag needs to fit within depending on the application. For example, RFID tags that are used for tracking need to be small enough to fit underneath the shipping labels of the product containers on which they are placed. For cases where the antenna has size constraints, tunable features like increasing the length of the antenna are not desirable. For these cases, either alternative ways of getting the antenna to have the desired electrical characteristics are needed, or poorer performance at some frequencies will have to be acceptable. There is ongoing research in the RFID field to find different ways of improving RFID tag antenna performance while keeping the antennas quite small.

7. Conclusion

The goal of this thesis has been to present the concept of designing planar T-match antennas to have frequency responses like 2nd-order Chebyshev band-pass filters. First, two different methods for analyzing the T-match antenna were presented. Both methods resulted in equivalent circuits for the T-match that had the same basic circuit form, and this form was shown to be that of a 2nd-order band-pass filter. Each analysis method also provided different insights into the behavior of the T-match antenna that can be used to manipulate the various electrical parameters of these antennas. Then, a Chebyshev filter was designed whose equivalent circuit and frequency response could be used as a target for those of a T-match antenna.

An existing commercial RFID tag antenna was redesigned to have a wider bandwidth with a power transfer efficiency response that behaved like a Chebyshev filter. The ALN-9562 RFID tag antenna was chosen for redesign because it has some of the more complex features of RFID antennas while still being simple enough to model in Ansoft Designer. Physical antenna features were discussed that were used to redesign the commercial antenna to match its frequency response to the target Chebyshev filter.

Three wideband antenna designs were achieved using different combinations of changes to the primary physical features of the antenna. For the first antenna design, as few geometric features of the commercial antenna as possible were changed to achieve a frequency response close to that of the target filter. The resulting geometry of this first antenna design had some undesirable characteristics though. Namely, there were large empty spaces between the T-section feed loop and the meanders of the antenna, and the port where the IC would attach sticks out below the rest of the antenna geometry. For the second antenna design, changing an

additional geometric feature resulted in an antenna geometry that no longer had the port sticking out below the rest of the antenna geometry, but still had large spaces between the T-section feed loop and the meanders. For the third antenna design, the meanders were shifted to a more centralized location between the T-section feed loop and the end patches, and the spacing between them was decreased to help correct for the undesirable effects from shifting them.

All three antenna designs were much more efficient than the original commercial antenna had been over the desired frequency range for world-wide RFID operation, increasing the efficiency from as low as -4 dB to only -0.5 dB across most of the frequency range. The increase in efficiency achieved by these antenna designs could allow them to be used effectively at longer distances than the antenna from which they were derived. If more read distance is not needed, then tags with more efficiency could be read with less transmission power needed from readers. This could potentially reduce the cost of readers. These wideband antennas may also be more useful to more countries than the original commercial antenna since their high-efficiency bandwidths are much wider. If more countries can use a tag, then there are potentially more customers to buy the tag and thus more potential income for the RFID tag manufacturer.

A major concern with the antenna designs in this thesis was that it was necessary to lengthen the antennas to achieve the desired electrical characteristics. Longer antennas may not be acceptable in a commercial environment, depending on the size constraints for the application in which the antenna is to be used. Given this, a valuable future step in this research would be to find a different way to lower the series resonant frequency.

There are at least two avenues of future follow-on work that would enhance this work. The first is more research into identifying other physical features of T-match antennas that could be used to change their electrical characteristics. It would be useful to have a variety of physical

features available to change so that antenna designs might be optimized for cost, ease of fabrication, size, or whatever the designer's primary concern may be.

The second area of suggested follow-on research would be attempting to apply the band-pass filter concept to antenna geometries other than the T-match. This could provide similar benefits to finding a variety of physical features that could be changed. It could potentially provide a variety of choices in antenna shape and size that designers could chose from to optimize their antennas for specific applications. For example, if a specific type of antenna works best for RFID tags attached to a certain material, the band-pass filter concept may be able to help make those tags readable from farther away.

8. References

[1] D. M. Dobkin, *The RF in RFID: Passive UHF RFID in Practice*. Burlington, MA: Newnes, 2008.

[2] D. D. Deavours, "Analysis and Design of Wideband Passive UHF RFID Tags Using a Circuit Model," *IEEE International Conference on RFID*, Orlando, FL, April 2009, pp. 283-290.

[3] S. Uda, *Yagi-Uda Antenna*. Tohoku University: Research Institute of Electrical Communication, 1954.

[4] C. Tai, "Theory of Terminated Monopole," *IEEE Transactions on Antennas and Propagation*, vol. AP-32, no. 4, pp. 408-410, Apr. 1984

[5] M. Hamid and R. Hamid, "Equivalent Circuit of Dipole Antenna of Arbitrary Length," *IEEE Transactions on Antennas and Propagation*, vol. 45, no. 11, pp. 1695-1696, Nov. 1997.

[6] K. R. Demarest and D. D. Deavours, "Limitations of the Uda Model for T-match Antennas," *Progress in Electromagnetics Research*, vol. 113, pp. 1-15, 2011.

[7] W. L. Stutzman and G. A. Thiele, *Antenna Theory and Design*. Hoboken, NJ: John Wiley & Sons, Inc., 1998.

[8] A. S. Sedra and K. C. Smith, *Microelectronic Circuits*. New York, NY: Oxford University Press, Inc., 2004.

[9] D. M. Pozar, *Microwave Engineering*. Hoboken, NJ: John Wiley & Sons, Inc., 2005.

[10] Impinj Inc, "Monza," 2006.

[11] Impinj Inc, "Monaco64," 2006.

[12] Alien Technology, "Higgs-3 Product Overview," July 2008.

[13] Impinj Inc, "Monza 3 Datasheet," 2008.

[14] Alien Technology, "Higgs-2 Product Overview," July 2008.

[15] Impinj Inc., "Monza 4 Tag Chip Data Sheet," 2010.

[16] EM Microelectronic, "EM4324," 2007.

[17] STMicroelectronics, "XRAG2," 2006.

[18] STMicroelectronics, "XRA00," 2004.

[19] Alien Technology, "ALN-9562 Squiggle-SH Inlay Product Overview," August 2008.